THE PENNSYLVANIA STATE UNIVERSITY
SCHREYER HONORS COLLEGE

DEPARTMENT OF BIOMEDICAL ENGINEERING

DETERMINING THE EFFECT OF KINESIN-5 ON THE NUCLEATION RATES OF MICROTUBLES IN VITRO AND SYNTHESIZING, CHARACTERIZING, AND PURIFYING FLUORESCENTLY LABELED NUCLEOTIDES

COLIN LINGAFELT
SPRING 2017

A thesis
submitted in partial fulfillment
of the requirements
for a baccalaureate degree
in Biomedical Engineering
with honors in Biomedical Engineering

Reviewed and approved* by the following:

William O. Hancock
Professor of Biomedical Engineering
Thesis Supervisor / Honors Advisor

Herbert H. Lipowsky
Professor of Biomedical Engineering
Faculty Reader

Justin L. Brown
Associate Professor of Biomedical Engineering
Faculty Reader

* Signatures are on file in the Schreyer Honors College.

ABSTRACT

Kinesin proteins are molecular motors in eukaryotic cells that have a variety of intracellular functions including transporting vesicle and protein cargo to different intracellular locations, and aiding in cell division. Motor proteins travel along microtubules to move across the cell using its two heads to "walk" along the filament. In order for a kinesin to "walk", it requires energy derived from ATP hydrolysis.

The first half of this thesis is dedicated to designing a protocol for synthesizing, purifying, and characterizing a fluorescently labeled nucleotide by reacting ATP with methylisatoic anhydride. The resulting mATP shows a peak absorbance around 356 nm and a fluorescence around 450 nm that is enhanced by motor binding. The purpose of labeling the nucleotides is to quantitatively study the kinesin chemomechanical cycle by measuring the on- and off- rates for nucleotide binding to the motor. From these data, more information can be discovered about the chemomechanical cycles for different kinesin variants. A cost analysis of producing mATP versus purchasing mATP determined that 85% of the cost can be saved by synthesizing the product in the lab instead of purchasing the same quantity from a commercial producer.

The second half of this thesis is dedicated to determining the effects of kinesin-5 motors on microtubule nucleation in vitro. Kinesin-5 (Eg5) is a tetrameric, mitotic kinesin that pushes apart antiparallel microtubules and helps to stabilize the mitotic spindle during mitosis. Because failure to complete mitosis can cause the cell to undergo apoptosis, Eg5 is a target for new cancer drugs that target rapidly dividing cancer cells. Eg5 was recently shown to enhance the microtubule growth rate in vitro, providing a new potential function of this motor as a regulator

of microtubule dynamics. Experiments were carried out using fluorescence microscopy and turbidity to measure the influence of Eg5 on microtubule nucleation in vitro. The fluorescence microscopy experiments showed a potential effect of Eg5 on nucleation but more data need to be collected before a definitive conclusion is made. The turbidity experiments did not show evidence that Eg5 affected microtubule nucleation. Therefore, the cumulative results of these experiments were inconclusive in determining whether Eg5 affects microtubule nucleation.

TABLE OF CONTENTS

LIST OF FIGURES

LIST OF TABLES

ACKNOWLEDGEMENTS

I would like to acknowledge, first and foremost, Dr. Hancock for being my advisor and mentor for the past two years. Your guidance, patience, and knowledge has not gone unrecognized. Thank you.

Next, I would like to acknowledge David Arginteanu and Geng-Yuan (Scott) Chen for their help in the development of this thesis project and their eagerness to help.

I would also like to acknowledge the NIH R01 GM076476 grant funding for their support to conduct a portion of this research that is presented in this thesis.

Lastly, I would like to dedicate this thesis to my family and all of the friends that I have made over the last four years. To the many memories that were, and the many that will be.

Chapter 1

Introduction

This thesis focuses on two separate projects that relate to different aspects of kinesin motor proteins. The first portion focuses on the development of a protocol for synthesizing, purifying, and characterizing mant-labeled nucleotides, and the second focuses on examining the effects of Kinesin-5 motors on microtubule nucleation in vitro. Both topics are related to current research in the field of molecular motors and this thesis introduces methodology for creating essential lab materials as well as innovative research to a question that has not been previously answered. Chapter 2 describes the methodology for developing the protocol to synthesize, characterize, and purify mant-labeled nucleotides. Chapter 3 investigates the changes of microtubule nucleation in the presence of kinesin-5 (Eg5) motors and will also provide insight on the potential effects of kinesin-5 inhibitors such as Monastrol, STLC, and BRD9876.

The synthetic work presented here is unpublished. The protocol has been implemented as a procedure for synthesizing mant-labeled nucleotides in the Hancock Lab at The Pennsylvania State University for use in a variety of experimental procedures. All the work presented here was based in part off of previous procedures published by Hiratsuka and Ni et al. [1], [2] as well as assistance provided by Dave Arginteanu.

The Eg5 work presented here was partly based on publications by Geng-Yuan Chen et al. (2017) [3], Zheng et al. (1995) [4], and Y. Chen and Hancock (2015) [5]. The experimental procedures that were performed were based on the results of microtubule shrinkage rate studies that compared different Eg5 inhibitors, microtubule nucleation dependence on γ-TuRC, and the

increased polymerization effects of microtubules in the presence of Eg5 as well as assistance provided by Geng-Yuan Chen.

1.1.1 Kinesin Motor Proteins

Kinesins are specialized motor proteins that are dependent on adenosine triphosphate (ATP) as an energy source, and they use ATP in order to facilitate transport of intracellular cargo along microtubules in eukaryotic cells along with other cellular processes depending on their particular function [6], [7]. There are many different families of kinesins, of which Kinesin-1 (KIF5A) is the most studied. Kinesin-1 is comprised of two motor head domains, making it a dimeric kinesin, that attaches directly to the microtubule and binds ATP [8]. A depiction of a traditional, dimeric kinesin structure is provided (Figure 1-1).

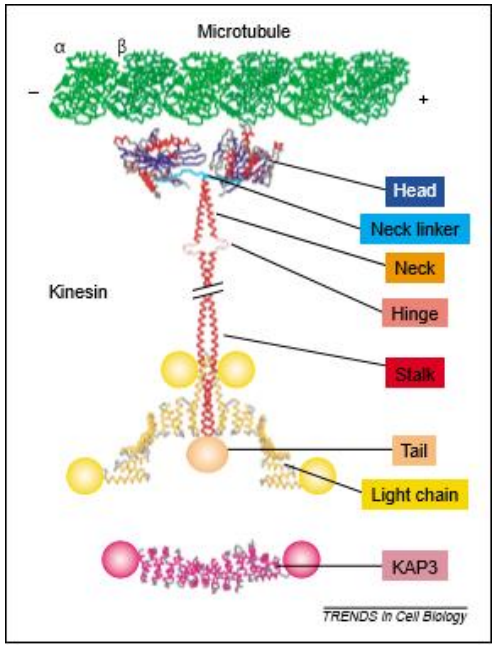

Figure 1-1. Model of a traditional dimeric kinesin. The figure displays components that are commonly seen throughout different kinesin variants. Figure adapted from [9].

Figure 1-1 shows a generalized model of a dimeric kinesin motor. Aside from the light chain, a kinesin motor contains a variable stalk that will change in length (by amino acid numbers) based on the kinesin's function. The hinge attaches the neck region to the stalk, and just like in a human, the neck connects the motor heads to the "body" of the kinesin. However, there is one additional feature to a kinesin that exists in the general anatomy. Kinesin motors contain a neck linker region that helps to attach the motor heads to the neck region. Finally, there are the motor heads of the kinesin which attach the motor to the microtubule [9].

These motor heads step processively towards the plus end of a microtubule in a "hand-over-hand fashion." This stepping process requires the energy of one ATP hydrolysis for each step [7,8,9]. The ATP hydrolysis / stepping cycle of kinesins will be discussed further in Section 1.1.3 of the Introduction.

1.1.2 Physiological Significance

There are many different families of kinesins that perform various functions. Kinesin-1 is involved in long distance transport within neurons to transport cargo like vesicles and proteins along axonal microtubules [10]. Many other families of kinesins are involved in the transport of proteins and other cargo. For example, kinesin-3 (KIF1A) is another type of axonal kinesin that is involved in the transport of synaptic vesicle precursors [7], [11]–[15]. Kinesin-2 (KIF3A/B) has a slightly different function within axonal transport; KIF3A/B is responsible for transporting fodrin-associated vesicles which aid in axonal elongation [16]. This process is essential for brain wiring. Additionally, kinesin-2 is also involved in bidirectional intraflagellar transport [17], [18]. Conversely, mitotic kinesins are a different subfamily of kinesins that are involved in

cellular division. Kinesin-5 (Eg5) is a mitotic kinesin that aids with separating the poles to form the mitotic spindle during mitosis [19]–[21]. There are many different kinesin motor proteins but all of them pertain to some type of important physiological role within the human body. Much is still uncertain about motor proteins like how their mutations cause physiological diseases or how their mechanisms work within the body. Researching these questions will lead to more informative knowledge about potential answers to these questions.

1.1.3 ATP Hydrolysis / Stepping Cycle

Kinesins require the energy from the hydrolysis of ATP in order to travel along a microtubule. Kinesin motors "walk" along a microtubule in a "hand-over-hand" fashion. In this analogy, the heads of the motor are analogous to feet that continually step forward, one after the other, taking steps of approximately 8.2 nm [22], as long as there is a constant supply of ATP present in the system. The process of a kinesin's stepping cycle can be seen in Figure 1-2. Each stepping cycle consists of the rear head detaching from the microtubule surface, the rear head moving past the bound front head, and rebinding to the microtubule in front of the leading head. This process requires the hydrolysis of one ATP molecule to ADP and the energy released allows the motor to carry out this process of movement. The net displacement of the overall kinesin molecule is approximately 8.2 nm, but the rear head has traveled a total distance of approximately 16.4 nm [23], [24].

This mechanism of processive stepping requires coordination between the two motor heads, and if this level of coordination is not achieved, then neither motor will be strongly bound to the microtubule surface and the motor will detach.

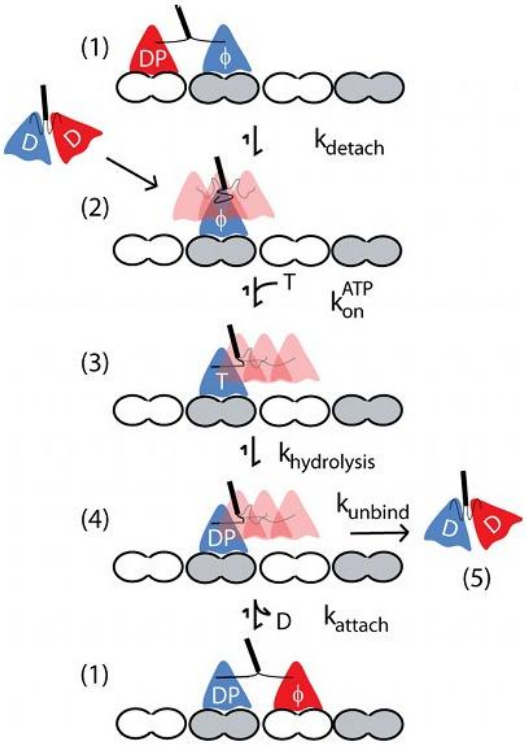

Figure 1-2. Model of chemomechanical hydrolysis cycle for a dimeric kinesin. The red and blue triangles represent the motor domain heads, the faded red triangles represent the motor diffusing forward, the black lines are the neck linkers of the motor protein which connects the heads to the stock. "T" denotes the ATP state, "DP" denotes the ADP and inorganic phosphate (Pi) state, "D" represents the ADP state, and "Φ" represents no-nucleotide bound. The cycle rates are defined by the rate constants given in the top right portion of each phase of the cycle. Figure was adapted from Kuty, Fricks, and Hancock (2010) [25].

In Figure 1-2, state 1 depicts a two-head bound state with a hydrolyzed ATP, in the ADP + P_i state, in the rear head and no nucleotide bound to the front head. When no nucleotide is bound to the motor, it induces a rigor-like state for the motor head which forces it to bind very strongly to the microtubule. The rear head is weakly bound to the microtubule so that it is capable of detaching and diffusing to the front which is depicted in state 2. ATP binds to the bound head in state 3 and is immediately hydrolyzed to the ADP + P_i state (state 4). After the motor reaches state 4 in the cycle, one of two things can happen. The bound head is now forced into a weak binding state so either the detached head has to release its ADP and bind to the microtubule (recycles to state 1), or the motor will detach.

This description of the kinesin mechanochemical cycle has generally been adopted by the science community as a consensus model of kinesin's motility [26]. It is the mechanism underlying this stepping process that has attracted researchers to the field and has developed new questions about how these motor proteins work as molecular machines and what roles they perform in cells.

1.1.4 Methylisatoic Anhydride - labeled Adenosine Triphosphate

The chemomechanical cycle depicted in Figure 1-2 is the basis for developing the protocol of synthesizing, purifying, and characterizing mant-labeled nucleotides. There are still many unresolved questions underlying the hydrolysis cycles of kinesins that need to be answered, such as how are the rates of nucleotide binding and release altered in diverse kinesins to alter their mechanochemical properties? One way of helping to quantify the ATP hydrolysis cycle is to fluorescently label the ATP or ADP nucleotides in the experiments so that the on- and off- rates of nucleotide binding can be monitored. Fluorescence is enhanced when mant-labeled nucleotides bind to motors as demonstrated in Cheng et al. (1998) [27]. Additionally, Chen, Arginteanu, and Hancock also showed that fluorescence is enhanced when mATP binds to the motor because quenching with water is reduced when the fluorophore is "protected" by the protein (hydrophobic environment of the binding pocket) [28]. Therefore, the use of these fluorescently labeled nucleotides will be very informative in future work for developing a better understanding of the hydrolysis cycles for different kinesins. This claim is supported by a few examples of researchers that have utilized fluorescently-labeled nucleotides in their experiments to quantify different parameters related to the kinesin mechanocycle. Stopped-flow is an

instrument used for measuring chemical kinetics by rapidly mixing two or more solutions and is frequently used to measure nucleotide binding and unbinding rates to motors. Patel et al. (2014), used mant-labeled nucleotides in their stopped-flow experiments to evaluate the turnover cycle of kinesins. The fluorescent nucleotides were being used to help visualize the rates at which kinesins spend their time within each step of the chemomechanical cycle. By doing so, the rate-limiting steps of the turnover cycle can be determined both in the presence and absence of microtubules [29].

Another example that demonstrates the practicality of fluorescent nucleotides is from Chen, Arginteanu, and Hancock (2015). In this article, researchers used fluorescent nucleotides to show that the movement of kinesin-2 is a result of rear head gating and not front head gating. This claim was achieved through stopped-flow and steady-state kinetics experiments in combination with single-molecule assays to characterize the kinetic cycle of kinesin-2. When attached to a microtubule, kinesin-2 would rapidly exchange mADP with mATP; however, when the motor was held in the 2 head bound state, the kinetics remained unchanged meaning that the rearward strain caused by this induced state did not affect the nucleotide binding in the front head of the dimer. Therefore, the fluorescent nucleotides were used to visualize the movement of the motor in the various states in order to help solve the question as to whether or not the motor was dependent upon its front or rear head being gated to the microtubule and to exhibit that fluorescence increases upon binding of mATP to kinesin-2 [28].

1.2.1 Microtubule Nucleation

The microtubule cytoskeleton is important for all eukaryotic cells because it has a significant role in mitosis and cytoplasmic organization. Microtubules are the largest component of the cytoskeleton and are long, hollow cylindrical structures with an average diameter of approximately 25 nm and length of tens of microns in some cases. Microtubules are composed of a collection of organized heterodimers called tubulin, each of which is comprised of an alpha subunit and a beta subunit [30]–[32]. Microtubule polymerization is a multi-step process that begins with microtubule nucleation. Microtubule nucleation is a process that initiates the growth of microtubules by combining tubulin subunits together in order to create a "seed" for the polymer to grow [33]. The process of nucleation occurs from an existing template of either a γ-tubulin ring complex (γ-TuRC) or a pre-existing microtubule [4]. γ-TuRC is a conical oligomer that has 13 γ-tubulins that are arranged in a ring. From this complex, microtubules can nucleate and grow [34]–[37]. Figure 1-3, adapted from Job, Valiron, and Oakley (2003), gives a representation on how microtubules can nucleate from a γ-TuRC.

Microtubule growth can occur in one of two ways. Either the tubulin subunits can connect longitudinally, which means that the heterodimers form long chains called protofilaments that extend the length of a microtubule. Alternatively, tubulin can attach laterally between the protofilaments. When lateral attachment occurs, alpha subunits connect to other alpha subunits and beta subunits connect to beta subunits to create a lattice-type structure which can stabilize the growing protofilaments on the microtubule. In this direction, the microtubule becomes fully cylindrical [38], [39].

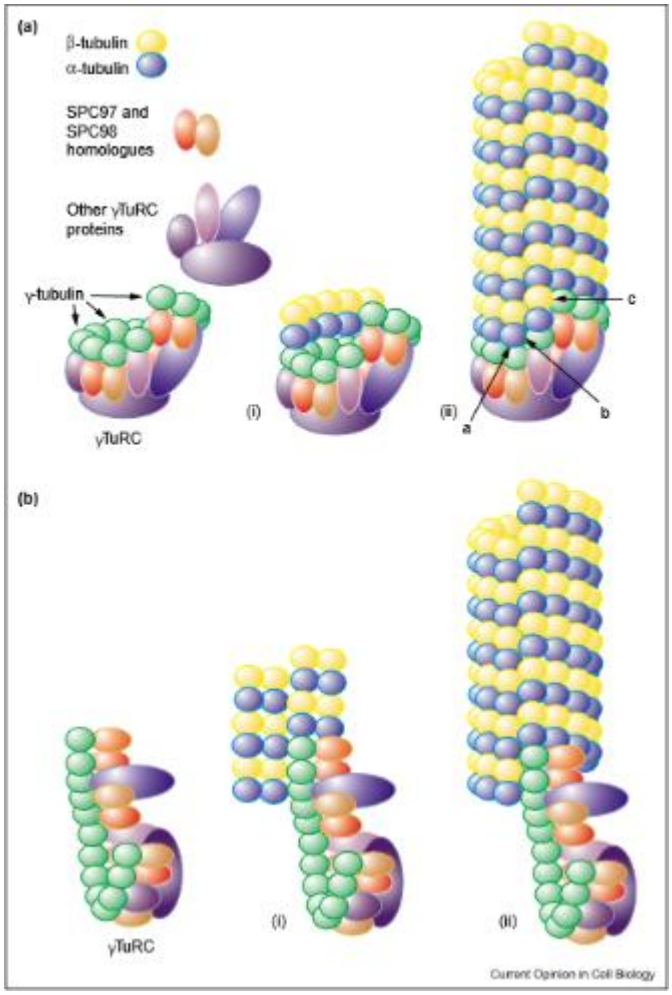

Figure 1-3. Models that illustrate microtubule nucleation using the γ-TuRC. a) Template model - the γ-TuRC mimics the end of a microtubule and tubulin dimers bind to the γ-tubulin proteins and grow radially outward. b) Protofilament model - tubulin dimers bind to the γ-TuRC, essentially creating a sheet of protofilaments that will wrap around and close once it becomes large enough. Figure adapted from Job, Valiron, and Oakley (2003) [40].

Figure 1-3 provides two separate models for microtubule nucleation on the γ-TuRC. The first illustration (Figure 1-3a) represents the template model in which γ-TuRC mimics the end of a microtubule and tubulin is able to bind to the γ-tubulin on the ring complex and grow radially outward form it. The template model gives the illusion of a spiral staircase being created but with a microtubule. The second representation (Figure 1-3b) illustrates the protofilament model

in which protofilaments are able to bind to the γ-tubulin of the ring complex and form a long sheet of connected tubulin dimers. Whenever the sheet becomes long enough, the tubulin will fold into its cylindrical, microtubule shape [40].

In correlation with the nucleation of microtubules on γ-TuRC, Zheng et al (1995) sought to quantify the dependence of γ-TuRC on the nucleation of microtubules. The purpose of the study was to establish that γ-TuRC affects microtubule nucleation. Figure 1-4 shows the numbers of microtubules that grew as a function of tubulin concentration present in the system. The microtubules were incubated both in the presence and absence of γ-TuRC in order to determine its effect [4].

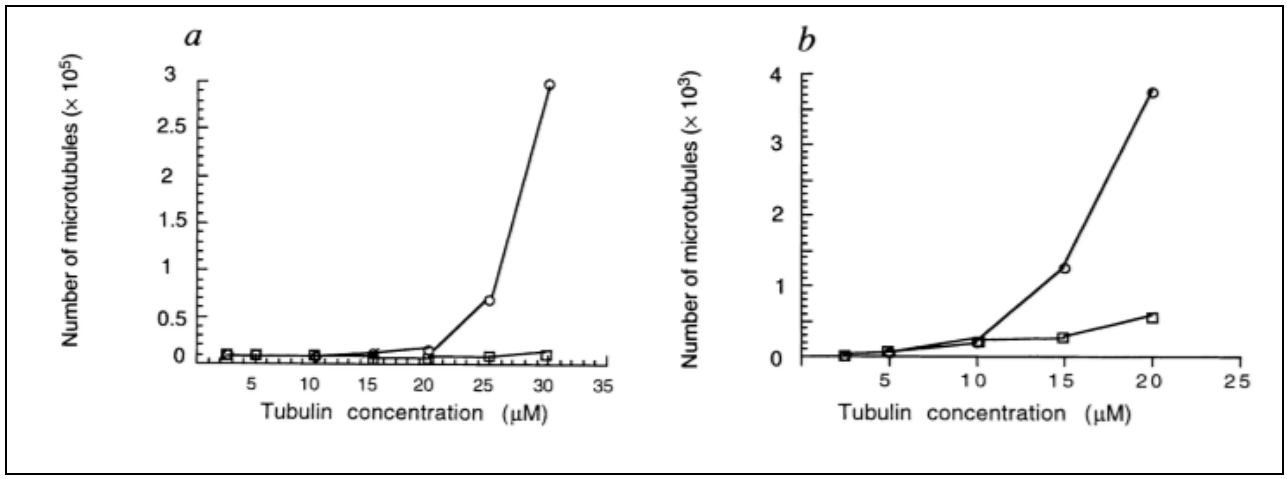

Figure 1-4. γ-TuRC's effect on the nucleation of microtubules. The microtubules that were grown in the presence of γ-TuRC are indicated by circles while the microtubules that were grown in buffer only are indicated by squares. a) shows the complete results for every concentration of tubulin that was experimentally tested, and b) shows the region of the results where the experimental begins to overtake the control. Figure adapted from Zheng et al. (1995) [4].

In Figure 1-4a, as the tubulin concentration is increased above 20 μM, the number of microtubules present increases drastically compared to the control group. The control group

does not show a substantial increase in growth as a result of higher tubulin concentrations. It can be inferred that the critical concentration for growing unseeded microtubules is beyond the 30 μM that is measured in this experiment. Figure 1-4b shows the region of the plot where the experimental group begins to outgrow the control group. It can be seen from this figure, despite the lack of error bars, that the critical concentration at which the γ-TuRC microtubules began to outgrow the control group is between 10 and 15 uM tubulin.

Recent work by Y. Chen and Hancock (2015) found that Eg5 can act as a microtubule polymerase and increase their polymerization rates while decreasing the rate of catastrophe [5]. Catastrophe is a term that describes an event when the rate of microtubule polymerization equals the rate of depolymerization which leads to the microtubule depolymerizing [41]. Figure 1-5 shows the process of microtubule growth as a function of time which helps to illustrate what a catastrophe event is [42], and Figure 1-6 summarizes their proposed kinesin-5 polymerase mechanism. In Figure 1-6, state 1 shows kinesin-5 walking towards the plus end of protofilaments where tubulin is binding reversibly. In state 2 and transitioning to state 3, if the motor steps before the newly added tubulin at the plus-end of the filament is able to dissociate, then any longitudinal interactions will become stabilized, slowing the rate of tubulin dissociation. This overall stabilization will enhance microtubule growth and reduce the chance of a depolymerization event. Over time, the growing protofilaments will be stabilized by lateral interactions and other protofilaments (state 4) to produce a long microtubule.

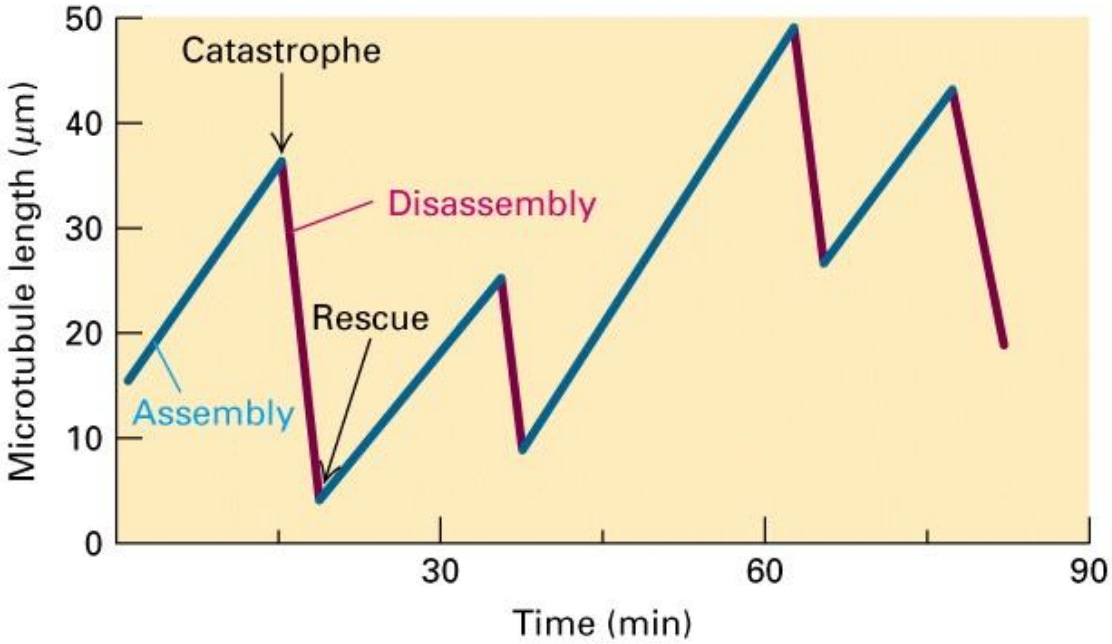

Figure 1-5. Dynamic Instability of Microtubule polymerization and depolymerization. The rapid process of microtubule growth is characterized by periods of assembly and disassembly. When a microtubule is about to change from polymerizing to depolymerizing, the brief moment of transition is defined as a catastrophe event. Similarly, when a microtubule is about to change from depolymzerization to polymerization, the transition is defined as a rescue event. Figure is adapted from [42].

These two articles pertaining to microtubule dynamics were summarized because the experiments performed in Chapter 3 aimed to combine the results of both publications and sought to show a relationship of dependence between Eg5 and microtubule nucleation.

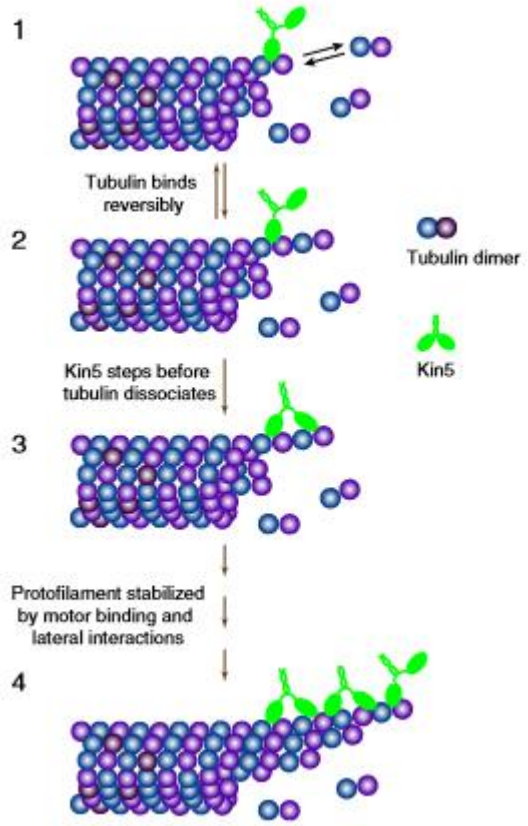

Figure 1-6. Proposed model of Kinesin-5 acting as a microtubule polymerase. Proposed model of microtubule stabilization as a result of Eg5 anchoring to the protofilament and acting like a polymerase which reduces the likelihood of a catastrophe event occurring. Figure was adapted from Y. Chen and Hancock (2015) [5].

1.2.2 Kinesin-5 (Eg5) Mechanism and Physiological Significance

Kinesin-5 is a mitotic kinesin that stabilizes the mitotic spindle during metaphase of mitosis. Eg5 has four motor heads, which defines it as a homotetrameric kinesin [19]–[21]. There are a few distinguishing factors that make Kinesin-5 different from the traditional kinesin-1. Eg5 walks with a tenfold slower velocity than KIF5A [43], [44], and is able to resist large mechanical loads (~ 10 pN) in either direction of resistance (with or against the direction of movement) [45], [46]. Eg5 stabilizes the mitotic spindle by sliding apart antiparallel microtubules during spindle formation in metaphase [19], [20]. This mechanical function leads

to the proper connection of the microtubule spindle fibers to the kinetochore of the chromosomes. Because of its critical functions in mitosis, kinesin-5 has become a prime target for anti-cancer pharmaceuticals [47]. The hallmark of human cancers is the presence of abnormal chromosomal numbers[48], [49], which is usually a direct result of a segregation error during cell division [50]–[52].

The end result is that a cancer cell still has active Eg5 motors that aid in cell division despite the cell having a chromosomal instability. This is an intriguing discovery for researchers that has led to the development of many anti-cancer therapies that will be discussed in the next section. In Chapter 3 of the thesis, some speculation will be provided within the discussion about how anti-cancer therapies could potentially affect microtubule nucleation.

1.2.3 Kinesin-5 Inhibitors

In an effort to develop more effective cancer chemotherapies, several classes of Kinesin-5 inhibitor drugs have been developed to treat patients with cancer. For this section, results will be quantitatively discussed from Chen et al. (2017) which provides some of the basis for the thesis research conducted in Chapter 3 [3].

The Eg5 inhibitors, Monastrol, STLC, and BRD9876, were quantitatively studied by Chen et al. to examine their affect on the binding state of kinesin-5 binding to microtubules [3]. In order to assess these inhibitors, Chen et al. performed mixed-motor gliding assays and measured the motor's velocity relative to a control value of 100 nm/s. Mixed-motor gliding assays are used to measure the speed of motors by tracking the rate of displacement of microtubules. For the study, a ratio of 22% Eg5 motors to 78% kinesin-1 HC (KHC) was used.

Chen et al. used kinesin-1 in the mixed-motor study to provide breaking ability when the motors are pulling so that the overall velocity would decrease. By doing so, more subtle changes in the velocity were able to be detected in the presence of inhibitors because the inhibitors prevent motility. The results of the study showed that Monastrol and STLC both increased the velocities of the kinesin-5 motors to approximately 300 nm/s and 350 nm/s respectively while BRD9876 decreased the motor's speed virtually to 0 nm/s. It was inferred from this data that both Monastrol and STLC both induce a weak-binding state to Kinesin-5 while BRD9876 induces a strong-binding state [3]. These results can be effectively seen in Figure 1-6. In addition to Monastrol and STLC, Ispinesib and Filanesib also induce a weak-binding state on the kinesin-5 motor.

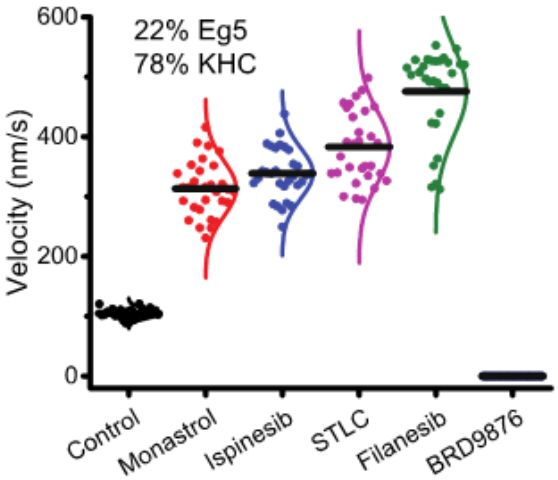

Figure 1-7. Kinesin-5 inhibhitors and their effects on kinesin-5 velocity. Mixed motor gliding assay results comparing the effects of kinesin-5 velocity in the presence of various kinesin-5 inhibitors. The black line that is present within the Gaussian fit for each inhibitor represents the mean motor velocity for that given condition. Figure borrowed from Chen et al. [3].

In correlation with the claims made by Chen et al. (2017), Groen et al. (2008) also developed a method to determine the effect of 2-(1-(4-fluorophenyl)cyclopropyl)-4-(pyridin-4-yl) thizaole (FCPT) on the binding state of Eg5. Groen et al. performed their experiment by

adding rhodamine-labeled Eg5 motors to a spindle assembly and using a spinning-disc confocal microscope to observe the overall "speckling," or brightness, of the motors. Next, FCPT was flushed into the system and the images were taken again. The results showed that the addition of FCPT substantially brightened the image because more motors were bound to the spindle fibers. The conclusion was that FCPT induced a strong-binding state upon Eg5 because a much higher percentage of the motors bound to the spindle assembly after the inhibitor was added [53]. The speckling of the FCPT image from the confocal microscope is shown in Figure 1-7.

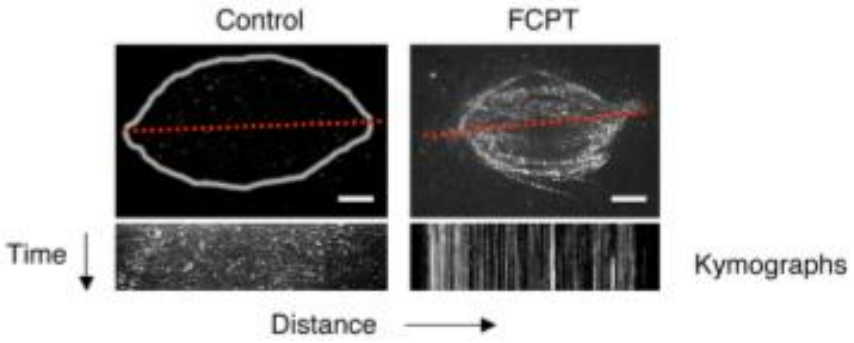

Figure 1-8. Kinesin-5 inhibitor speckling study. Resulting images from Speckling study that was performed in order to examine FCPT's effect on the binding state of kinesin-5 as an inhibitor. The top two images show the mitotic cells that were observed under the microscope and the bottom two images are the Kymographs corresponding to the above images. The figure was borrowed from Groen et al. [53].

An example of an *in vivo* study of Eg5 inhibitors (Skoufias et al. 2006) showed their potential as anti-cancer chemotherapies by studying the effects of the mitotic progression of STLC. The paper tested the effects of adding STLC to dividing HeLa cells. Both the control and the experimental groups were expressing GFP-α-tubulin so that they could be imaged and tracked during their mitotic progression. The control group successfully reached cytokinesis in 50 minutes. The dwell time for the cell to form a bipolar spindle was 10 minutes, and the cell reached anaphase within 35 minutes. The STLC treated cell initially saw the creation of two

distinct centrosomes, but they never separated more than 2.9 um apart. Therefore, the cell never fully separated and carried out the processes of mitosis. The reported result was that the initial separation of the centrosomes appeared but all recorded cells collapsed inward onto the monastral spindle [54]. The potential functionality of STLC as an anti-cancer chemotherapy is demonstrated by this *in vivo* study.

In a separate study, Chen et al. measured the microtubule shrinkage rate as a function of Eg5 inhibitors. The experimentally measured results were compared to a control shrinkage rate for a depolymerizing microtubule. The experiment was performed by binding Cy5-labeled, taxol-stabilized microtubules to a coverslip. Next, the taxol was washed out in order to induce depolymerization and the rate was measured. As seen in Figure 1-8, the control rate of shrinkage was 4.10 ± 1.10 nm/s, and upon adding Eg5 motors to the system, the depolymerization rate decreased to 2.90 ± 0.70 nm/s because kinesin-5 helps to stabilize microtubules [5]. When different Eg5 inhibitors were added to the system, such as Monastrol or BRD9876, the shrinkage rates changed substantially. Monastrol increased the shrinkage rate to about 4.5 ± 1.10 nm/s because it induces a weak-binding state of Eg5 while BRD9876 forced the depolymerization rate to drop to 0.66 ± 0.36 nm/s because of its ability to induce a strong-binding state on kinesin-5. Therefore, the microtubule depolymerizes at a very slow rate relative to normal conditions when BRD9876 is present [3].

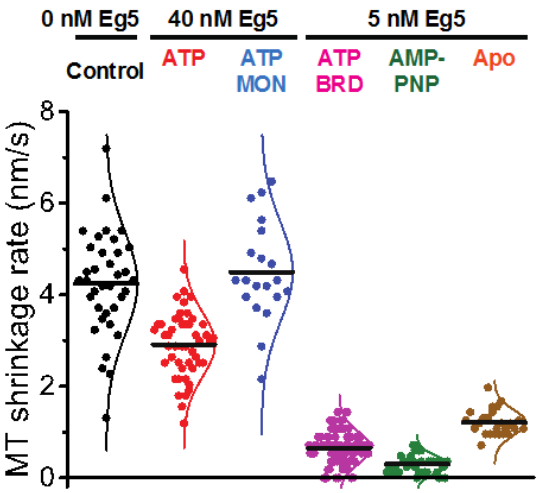

Figure 1-9. Effect of kinein-5 inhibitors on microtubule shrinkage rate. Inhibition assays to determine microtubule shrinkage rate as a function of Eg5 inhibitor. The black line that is present within the Gaussian fit for each condition represents the mean microtubule shrinkage rate. Figure was adopted from Chen et al. [3].

The previous work presented in relation to kinesins, it's chemomechanocycle, and fluorescent nucleotides provides the basis for Chapter 2. Chapter 2 outlines the Methods, Results, and Discussion for a developed protocol to synthesize, purify, and characterize mant-labeled nucleotides. In addition, the previous work on Kinesin-5, its physiological significance, microtubule kinetics and kinesin-5 inhibitors lays the foundation for Chapter 3. In this chapter, experiments were conducted to help answer the proposed question as to whether or not Kinesin-5 changes the nucleation rate of microtubules. Speculation will be provided within the Discussion section of Chapter 3 on kinesin-5 inhibitors and their effects on the nucleation rates of microtubules. Chapter 4 is the Conclusion Chapter that will summarize all of the supported claims that were made within the previous two chapters.

Chapter 2

Protocol for Synthesizing, Characterizing, and Purifying Mant-Labeled Nucleotides

The synthetic work presented here is unpublished. The protocol has been implemented as a procedure for synthesizing mant-labeled nucleotides in the Hancock Lab at The Pennsylvania State University for use in a variety of experimental procedures. All the work presented here was based in part of previous procedures published by Hiratsuka and Ni et al. [1, 2] and was carried out with the assistance of David Arginteanu. Chapter 2 provides the methods and related results for synthesizing, purifying, and characterizing mant-labeled adenosine triphosphate (mATP). A discussion is also provided to explain the results present and the written Standard Operating Procedure (SOP) for the Hancock Lab is supplied in Appendix A.

2.1 Materials and Methods

2.1.1 Synthesizing mant-labeled ATP

1 mmol of 5'-adenosine-triphosphate (Thermofischer Scientific, Molecular Weight = 551.15 g/mol) was dissolved into 15 mL of distilled water along with 1.50 mmol of methylisatoic anhydride (TCI, Molecular Weight = 177.16 g/mol). The pH of solution was then adjusted to 9.6 with 2M NaOH, and the mixture was placed in an incubator at 37$^{\circ C}$ for 2 hours and shaken at 250 rpm. The pH of the solution was checked every 20 minutes using pH indicator strips and the pH was readjusted to 9.6 by adding more 2*M* NaOH if necessary.

Following incubation, the pH of the solution was adjusted to pH 7 by adding 1M HCl. The sample was then stored in a freezer at -10°C until ready for purification.

2.1.2 Purifying mant-labeled ATP via Anion Exchange Chromatography

The crude mant-labeled ATP solution was purified using a DEAE-Sephadex Anion Exchange column (GE Healthcare) via a linear gradient buffer of triethylammonium bicarbonate (EMD) over a 50 mL drip volume, Low salt = 5 mM, High salt = 900 mM. Each buffer solution had the pH adjusted to 8.5. The unpurified sample was injected into the FPLC system after the column had been equilibrated with low salt buffer. The injection volume of sample was 1.50 mL and was collected in sequential 1 mL fractions over a 50 mL drip volume. The software for running the column was a preloaded program developed in Unicorn that charges up the column with the low salt buffer, then linearly increases the salt concentration over the 50 mL drip volume in a linear gradient.

2.1.3 Characterizing mant-labeled ATP via UV-VIS spectroscopy

The 1 mL fractions collected from the Anion exchange column were then tested for absorbance at the wavelengths of 250 nm and 356 nm using a UV-VIS spectrophotometer (HP Agilent 8453A) via a quartz cuvette with a path length of 1 cm. The specific wavelengths of 250 and 356 nm were chosen because each of these peaks corresponds to the maximum absorbance of unlabeled and mant-labeled ATP respectively. The ratio of significance (A250 nm / A356 nm) in which a single mant-group is bound to an ATP molecule was defined from literature as

any ratio greater than 3.50 being the desired product [2]. The extinction coefficient for mATP is 23 mM^{-1} cm^{-1} at a wavelength of 250 nm and 5.80 mM^{-1} cm^{-1} at a wavelength of 356 nm [55].

2.1.4 Characterizing mant-labeled ATP via Fluorescence Spectroscopy

After distinguishing the fractions as either mant-labeled or unlabeled ATP and quantifying the concentration of the labeled samples, fluorescence was measured in order to further characterize the mATP samples. The data were measured as an emission spectrum between 300 and 600 nm on a spectrofluorimeter (Shimadzu) with an excitation wavelength of 356 nm. The fluorescence spectrum was first taken with just the mant-labeled nucleotides diluted to 10 μM in a buffer of BRB-80, and this sample was used as the reference spectrum. Next, KIF3A560GFP (kinesin-2, fluorescently labeled with a GFP) motors [28] (25 nM) were added to the solution and the spectrum was measured again. A significant increase in the fluorescence spectrum around 450 nm was indicative of mATP binding to the motors. The GFP signal did not interfere with the mATP signal because the peak fluorescence for the GFP was measured around 525 nm.

2.1.5 Characterizing mant-labeled ATP via kinetic measurements

Kinetic data were generated via using the kinetics mode on the spectrofluorimeter used in 2.1.4. The experiment was set up by placing 1 μM of mATP into BRB-80. The fluorescence intensity was measured for 1000 seconds at its current state, then about 50 nM of KIF3A (kinesin-2) motors were flushed into the system, and the fluorescence was measured continuously for another 1000 seconds. Finally, 1 μL of 100 mM unlabeled ATP (1 mM) was

added to the system so that the mATP would unbind from the motor and the intensity was again measured for another 1000 seconds while steady-state was reached. The exponential curves obtained were fitted to a single exponential in MATLAB via the curve-fitting tool. The values of k_{on} and k_{off} were determined from the exponential fits.

2.2 Results

2.2.1 Synthesis and Purification of mant-labeled Nucleotides

For the synthesis of mant-labeled nucleotides, the initial procedure followed the methods of Hiratsuka (1983) [1]. Following the synthesis procedure, the products were purified via a DEAE Sephadex Column using a linear gradient of a triethylammonium bicarbonate buffer as outlined in Ni et al. (2000) [2]. The resulting chromatograph for the purification process was measured at a wavelength of 280 nm and is shown in Figure 2-1.

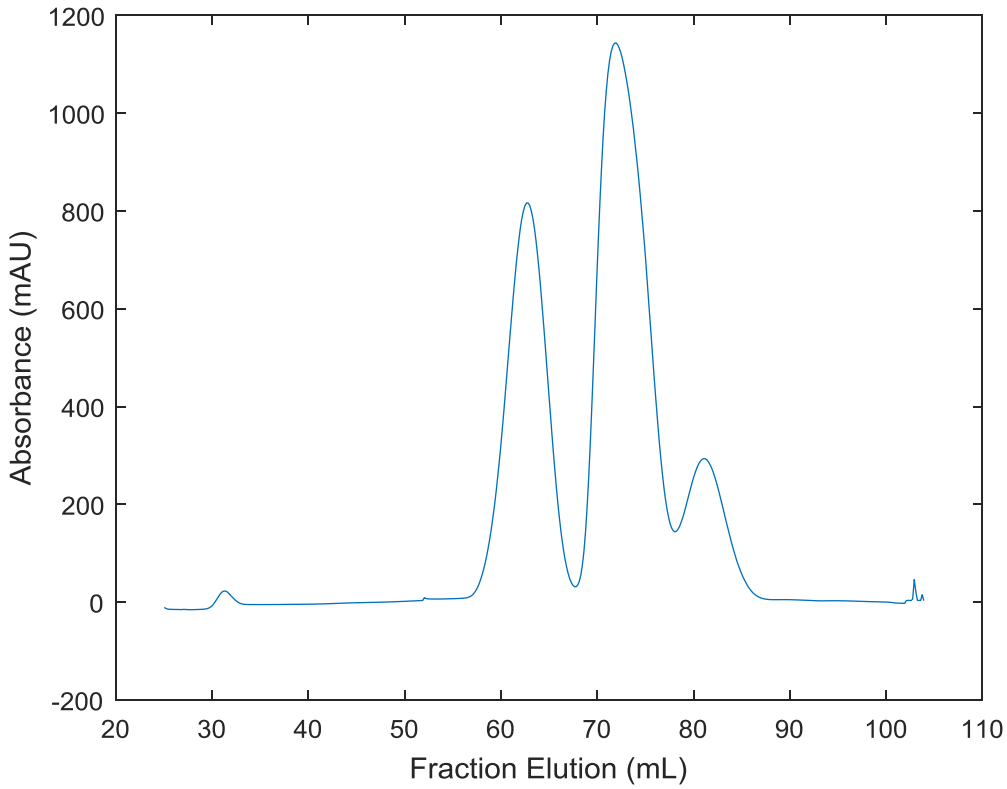

Figure 2-1. DEAE Chromatograph of mant-labeled ATP purification from 2015. The sample volume loaded into the column was 1.50 mL. The absorbance value at which this chromatograph was measured was 280 nm.

The chromatograph shown in Figure 2-1 has three distinct peaks. Upon analyzing these chromatograph peaks via UV-VIS Spectroscopy, it was resolved that the first peak in the chromatograph was un-reacted methylisatoic anhydride (mant). The second peak was identified as unlabeled ATP, and the third and smallest peak in the chromatograph was identified as mant-labeled ATP, or the product of interest. Therefore, it was determined that the reaction did not proceed well in the forward direction.

Unsatisfied with the resulting yield of products, several factors were tested in an attempt to improve the reaction yield including pH balance, stoichiometry, and reaction time, and

reaction temperature. The distinguishing factor that drove the reaction completion was maintaining the pH around 9.6 during the synthesis reaction (Section 2.1.1). Therefore, pH test strips were used to test the solution every 20 minutes during the reaction procedure. The pH was then adjusted accordingly based on the reading taken whether acid or base needed to be added. The resulting products were purified by the same process according to Ni et al. (2000). The resulting chromatograph for the modified synthesis procedure was measured at a wavelength of 280 nm and can be viewed in Figure 2-2.

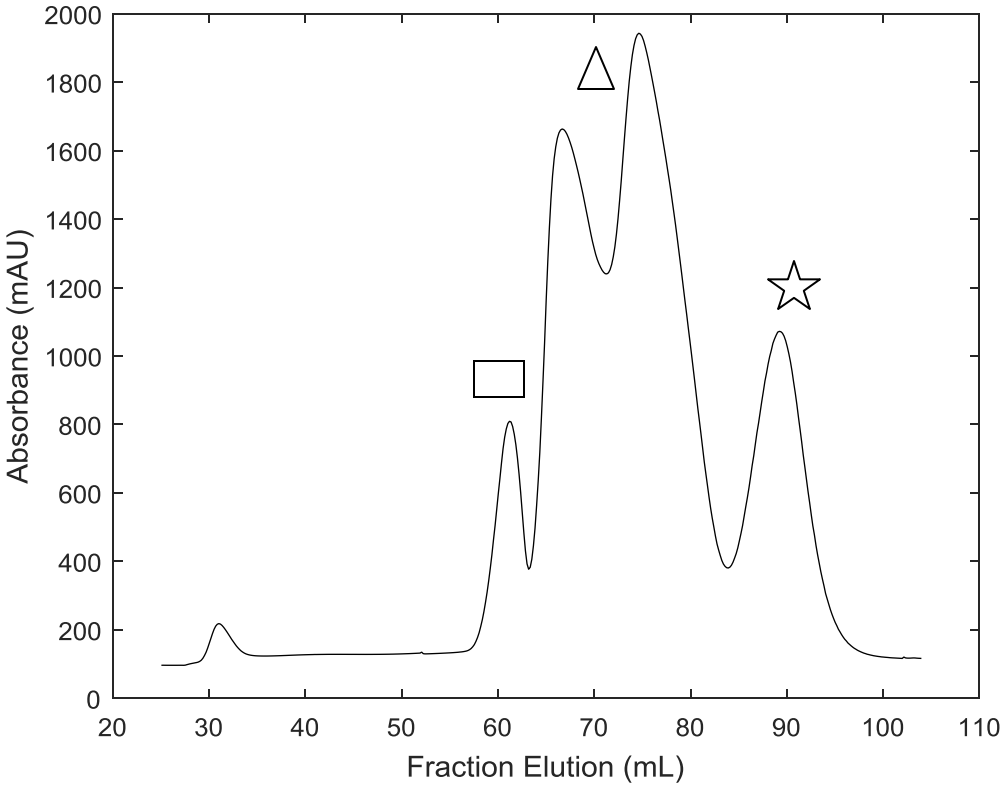

Figure 2-2. DEAE Chromatograph of mant-labeled ATP purification from 2016. The sample volume loaded into the column was 2.0 mL. The chromatograph was measured at a UV wavelength of 280 nm. The peak next to the rectangle was determined to be un-reacted mant, the two peaks that are closest to the triangle are unlabeled ATP, and the peak that is closest to the star is mATP.

One point to note about the chromatograph in Figure 2-2 is that the column was loaded with a sample volume of 2.0 mL for this purification as where the sample volume loaded in Figure 2-1 was only 1.5 mL. However, it is clear from the figure that the sample resolved into 4 distinct peaks. After analyzing these signals by UV-VIS Spectroscopy, the peak with the rectangle next to it was identified as un-reacted metylisatoic anhydride. The two peaks that are next to the triangle were identified as unlabeled ATP, and the peak next to the star was the product of interest, mATP.

Examining the different chromatographs in Figures 2-1 and 2-2, the resolution of the mATP peak is much better in Figure 2-2. The resolution is being evaluated in a qualitative sense because the separation between the unlabeled ATP peak and the mATP peak is larger in Figure 2-2 than it is in Figure 2-1. To help justify this observation, the chromatographs were superimposed and plotted together in Figure 2-3.

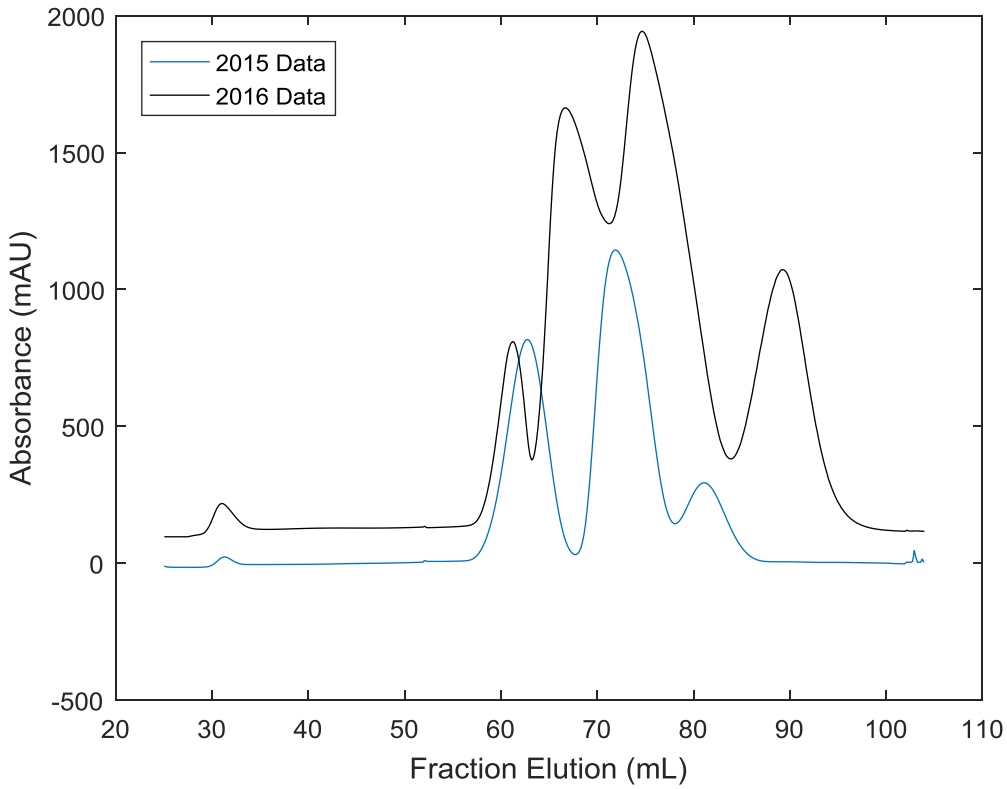

Figure 2-3. DEAE Chromatograph of Figures 2-1 and 2-2 superimposed. The blue curve shows the chromatograph from Figure 2-1 and the black curve shows the chromatograph from Figure 2-2.

From examining the chromatographs in Figure 2-3, it is apparent that the signals overlap to some extent. But the more interesting comparison, because the loading volumes are not consistent, is the ratio of mant-labeled ATP to the unlabeled ATP. For the 2015 data, the value approximates to 300/1150 ≈ 0.261. For the 2016 data, the value approximates to 1100/1950 ≈ 0.564.

2.2.2 Characterization of Mant-Labeled Nucleotides via UV-VIS Spectroscopy

In order to characterize the signal peaks from the chromatographs in Figures 2-1 and 2-2, UV-VIS spectroscopy was used as the primary step for determining the identity of the product fractions that eluted from the column. To distinguish the unlabeled nucleotides from the labeled nucleotides, the ratio of absorbance between 250 nm and 356 nm was calculated. If the ratio resulted in a value that was ≥ 3.50, then this sample was regarded as a singly-labeled mant-nucleotide. This procedure was adopted form Ni et al. (2000) [2].

However, in order to compare the results of the synthesized sample to a reference value, a sample of purchased mATP from Thermo Fisher at a known concentration of 100 uM was diluted and analyzed using the same instrument. The results of the UV-VIS Spectral Analysis are given in Table 2-1. Further details about this procedure can be found in Section 2.1.3. It is apparent from the results given in Table 2-1 that the synthesized sample is relatively equivalent with the commercial grade product when compared in terms of absorbance spectra.

Table 2-1. Summary of UV-VIS Spectrophotometer Data. The data are comparing a commercially synthesized product to newly synthesized products.

Sample (Rel. Conc.)	Absorbance at 250 nm	Absorbance at 356 nm	Ratio A250/A356
Sigma Aldrich Sample (≈25 uM)	0.609	0.169	3.61
Synthesized Sample (≈25 uM)	0.680	0.174	3.91

2.2.3 Characterization of Mant-Labeled Nucleotides via Fluorescence Spectroscopy

In addition to UV-VIS spectroscopy, fluorescence spectroscopy was also employed. In this test, approximately 10 µM of the synthesized mATP nucleotides was excited at a wavelength of 356 nm and the resultant emission spectrum was observed between 300 and 600 nm. This experiment was first done in the absence of KIF3A560GFP (kinesin-2) motors. Next, kinesin-2 motors (25 nM) were added to the system and the spectrum was measured again to see if an increase in fluorescence was observed. The fluorescence spectrum is shown in Figure 2-4. Kinesin 2 was used for this particular experiment because it has a higher affinity for mATP than it does for unlabeled ATP [28]. Further details about the specifics of this procedure can be found in Section 2.1.4.

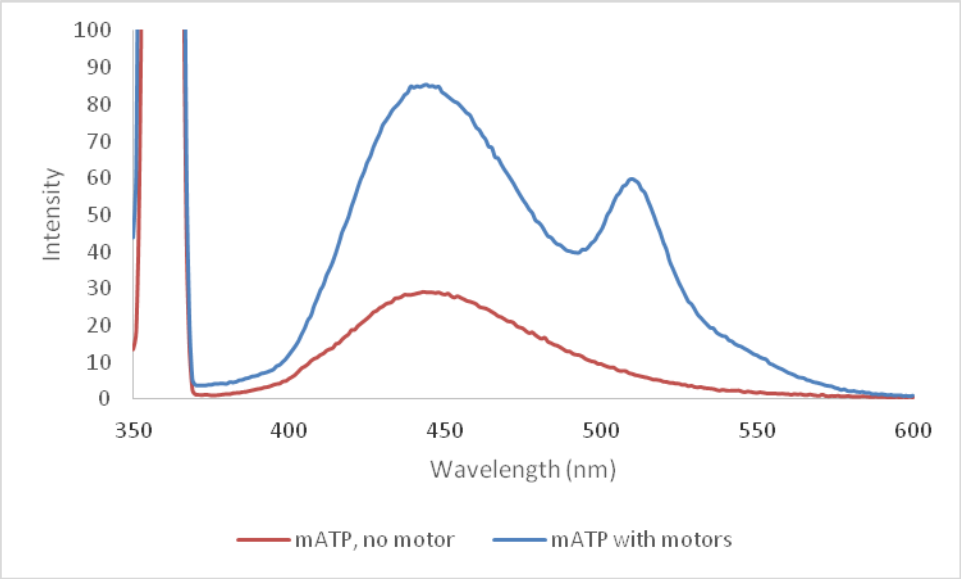

Figure 2-4. Fluorescence Data of 10uM mATP. The excitation wavelength was set to 356 nm and the emission spectrum was measured from 300 to 600 nm. The spectrum shown here only depicts the spectrum from 350 to 600 nm. The spectrum of mATP was first measured in the absence of Kinesin-2 motors (red) and then a concentration of 25 nM KIF3A560GFP (Kinesin-2) motors was flushed into the system and the spectrum was measured again (blue). The second resulting peak at a wavelength of about 520 nm is the fluorescence given off from the GFP.

Figure 2-2 demonstrates that the fluorescence of the mATP at 450 nm increases approximately threefold after kinesin-2 motors have been added to the system. The second resulting peak around 520 nm is a product of the GFP from the kinesin motors.

2.2.4 Characterization of Mant-Labeled Nucleotides via Reaction Kinetics

Lastly, the mant-labeled nucleotides were further characterized by determining the reaction rates of binding to molecular motors. For the kinetics experiment, kinesin-2 motors (KIF3A) were placed in buffer with a low amount of ATP (~ 50 nM). The motors were monitored over a period of 1000 seconds while they reached a steady-state. The excitation wavelength was 356 nm and the intensity of the signal was measured at 450 nm. Next, 1 μM mATP was flushed into the system and the binding rate was measured over an interval of another 1000 seconds. Lastly, 1 μL of 100 mM ATP (1 mM) was added to solution to cause the mATP to unbind from the motors. The third interval of 1000 second was used to measure the unbinding rate. The resulting intensity plot for this experiment is shown in Figure 2-5.

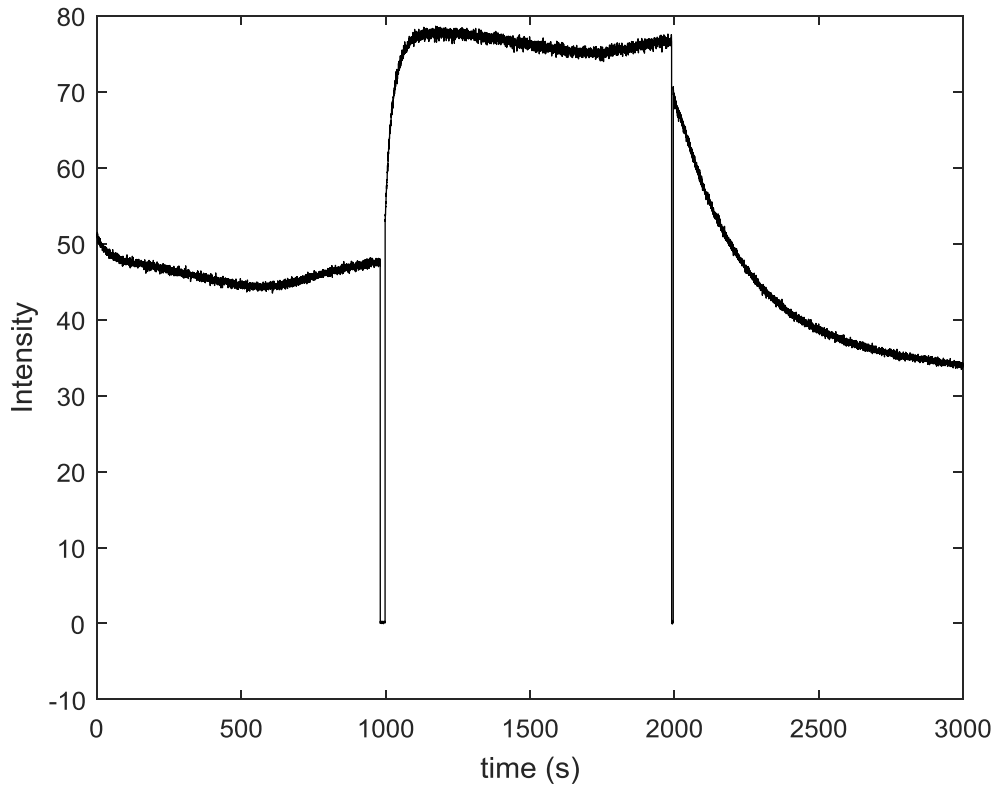

Figure 2-5. mATP kinetics experiment. Results from kinetics data experiment to determine the binding and unbinding rate of mATP. Intensity was measured vs. time at a wavelength of 356 nm. mATP was placed into solution and kinesin-2 motors or unlabeled ATP were added to the system. Each phase of the experiment was evaluated over a period of 1000 seconds. For $0 < t < 1000$, the steady state intensity was measured (no motors), then for $1000 < t < 2000$, kinesin-2 motors were added to the solution at the beginning of the interval and the system was measured as the intensity changed, and from $2000 < t < 3000$, unlabeled ATP was added to the solution at the beginning of the interval and the intensity change was measured.

Figure 2-5 shows 3 distinct regions of activity that correspond with the changing conditions imposed upon the system. The first interval (0 to 1000s) shows the steady-state kinetics with nucleotide binding. The second interval (1000 to 2000s) after the addition of kinesin-2 shows an exponential rise which corresponds to the binding of mATP to kinesin-2. The third interval (2000 to 3000s) after the addition of unlabeled ATP shows an exponential

decay of the mATP unbinding. The data in the exponential regions was extracted and each curve was fit to a single exponential. The curves are shown below in Figures 2-6a and 2-6b.

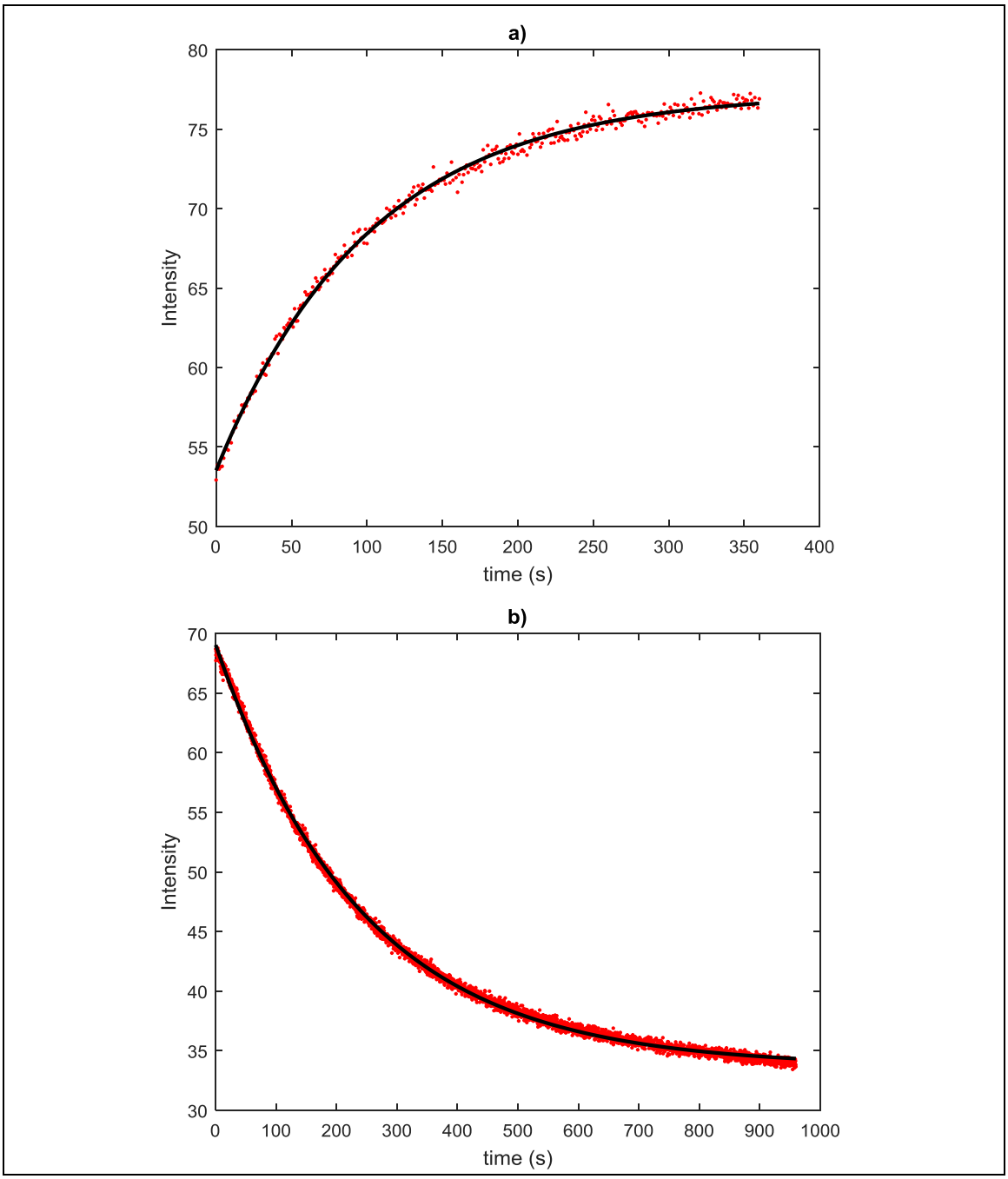

Figure 2-6. mATP kinetics experimental data curve fits. After the kinetics experiment was completed, the data from the experiment were extracted and the regions immediately after the mATP or unlabeled ATP were added were plotted in MATLAB, a) binding of mATP, b) unbinding of mADP. The curve fitting tool was then used to fit a single exponential to each function in order to determine the binding and unbinding rate of the mATP.

The exponential function fitted to Figure 2-6a is given in Equation 1, and the exponential coefficient is defined as the unbinding rate of unlabeled ADP which quantitatively defines the rate of mATP binding because mATP binds to the motor much faster than the unlabeled ADP can dissociate.

$$y = -23.77e^{-(0.009851x)} + 77.30 \quad (1)$$

Therefore, the calculated binding rate for the kinetic data is approximately 0.01 s^{-1}. The unbinding rate of mADP can be determined from the exponential coefficient that characterizes the mADP unbinding equation. The exponential function fitted to Figure 2-6b is given in Equation 2.

$$y = 35.36e^{-(0.00415x)} + 33.68 \quad (2)$$

Hence, the unbinding rate for the kinetic data is approximately 0.004 s^{-1}. Chen, Arginteanu, and Hancock (2015; Figure 3 legend), reported a binding rate for mATP to Kinesin-2 of 0.03 s^{-1} and an unbinding rate of 0.002 s^{-1} [28]. The experimentally determined values have the same order of magnitude in comparison to the values found in literature.

2.3 Discussion

The results presented in Sections 2.2 - 2.5 cumulatively support the claim that the synthesized product, developed according to the procedures outlined in Section 2.1, is mant-labeled adenosine triphosphate (mATP). The results in Section 2.2 demonstrated that the methods provided by Hiratsuka (1983) and Ni et al. (2000) generate mATP but in a very low yield. This claim is evidenced by the small product signal peak that appears in Figure 2-1.

Furthermore, the ratio of the product signal to the unlabeled ATP signal yielded a value of approximately 0.261, which can be interpreted as only 1 ATP molecule is being labeled for every 4 that are not. Upon analysis of the experimental procedure, it was discovered that maintaining a pH of 9.6 during the synthesis reaction produces a much better yield. This claim is evidenced by the chromatograph given in Figure 2-2 and the superimposed figure of both chromatographs in Figure 2-3. The reaction is believed to change the pH of the solution during its progression because carbon dioxide is produced in the proposed synthesis mechanism. Because carbon dioxide is produced in the presence of water, the carbon dioxide will react with the water to create carbonic acid which will then dissociate into bicarbonate and a proton. The proton will make the pH of solution more acidic. Because of this reaction change, the constant addition of base is needed to keep the pH constant.

In Figure 2-2, it is apparent that the mATP signal contains a much better separation from the unlabeled ATP peak than it does in Figure 2-1. Furthermore, the ratio of product signal to unlabeled ATP signal yielded a value of approximately 0.564. This value can be interpreted as 1 ATP molecule being labeled for every 2 that are not. Compared to the original procedure, the modifications to the synthetic procedure practically doubled the efficiency of the reaction.

The use of UV-VIS spectroscopy was employed as an identification tool following the purification process. The guidelines specified within Ni et al. (2000) recommended that a singly-labeled mant-nucleotide was identified when the ratio of absorbance of the nucleotide to the mant-group was ≥ 3.50. This guideline was used in the present work. After identifying the mant-labeled nucleotide samples, the absorbance data was compared to a commercial grade product to determine its purity. The results of this analysis were summarized in Table 2-1. The synthesized product presented in this thesis had a slightly higher ratio than the commercial grade

product. Because a large enough sample size is not present, it cannot be said that the synthesized product is of better quality than the commercial grade product, but it can be said that the synthesized product is of the same nature as the commercial product since the contents of the commercial product is 99% pure.

The fluorescence and binding kinetic data that were shown in Figures 2-4 through 2-6 further support the claim that the product synthesized was mATP. The fluorescence data in Figure 2-4 clearly showed that an increase in fluorescence was present from exciting the mant-labeled nucleotides at a wavelength of 356 nm and measuring the emission spectrum from 300 to 600 nm. It is known that when mATP is attached to a Kinesin-2 motor, the fluorescence of the nucleotide will increase [28]. Therefore, it was important to establish a reference spectrum for the nucleotides so that a change in fluorescence could be observed after adding the kinesin motors. The peak fluorescence wavelength occurred around 450 nm and increased by threefold upon adding kinesin-2 motors. The mATP binding kinetics data also showed positive results that were related to literature values. The purpose of performing the kinetics experiment was to determine the binding and unbinding rate of the mATP/mADP to kinesin-2. The binding and unbinding rates were 0.01 s^{-1} and 0.004 s^{-1}, which are within the same order of magnitude as the literature values of 0.03 s^{-1} and 0.002 s^{-1} respectively [28]. The noisy signal that was measured from the insensitive instrument could have caused some of the discrepancy in the results. The binding rate measurement is actually measuring the unbinding of unlabeled ADP because ADP unbinds from the motor at a much slower rate than mATP binds to the motor [28]. Therefore, it is difficult to quantitatively compare experimental rates because there are sources of uncertainty that can contribute to the difference in the quantified values. Conversely, the unbinding rate is more sensitive because a direct measurement is being observed. However, the literature value

may differ because the results were fit to a bi-exponential function while the data presented were fitted to a single exponential. If this experiment were to be repeated using a stopped-flow device, the binding and unbinding rates may result in more accurate values.

Therefore, all of the data presented here support the claim that the synthesized product is mant-labeled adenosine triphosphate (mATP). In addition, a cost analysis was performed to determine the productivity of performing the synthesis procedures in the lab compared to purchasing the nucleotides from an industrial supplier. The cost of materials and buffers for synthesizing 8 µmol of mATP is approximately $160. The cost of purchasing the same mass of mATP from Sigma Aldrich is approximately $1,120. Therefore, the cost savings of producing mATP is about 85.7%. The procedures and evidence used to support this claim has been accumulated into a Standard Operating Procedure (Appendix A) that has been implemented into practice within the Hancock Lab at The Pennsylvania State University.

Chapter 3

Determining the Effects of Eg5 on Microtubule Nucleation

The microtubule nucleation methods used here were partly based on publications by Chen et al. (2017) [3], a publication about the tubulin dependence of microtubules by Zheng et al. (1995) [4], and a publication about the polymerizing effects of Eg5 on microtubules Y. Chen and Hancock (2015) [5]. The experimental procedures performed were based on the procedures developed in the Hancock Lab at the Pennsylvania State University and assistance in developing the procedures was provided by Geng-Yuan Chen. The question addressed was whether Eg5 has an effect on the nucleation of microtubules. This question was addressed in two separate ways: microscopy experiments using an upright TIRF microscope and kinetics experiments using a PlateReader.

3.1 Materials and Methods

3.1.1 Polymerizing rhodamine-labeled microtubules

Experimental procedures are described for polymerizing 20 µM rhodamine-labeled tubulin. This procedure was repeated numerous times in order to polymerize microtubules in varying concentrations of tubulin. When the procedure was adapted for the changing concentrations of tubulin, the volume of BRB-80 added to solution increased or decreased in

order to compensate for the changes in tubulin volume so that the consistent total volume was 10 µL.

5 µL of 40 µM rhodamine-labeled tubulin, 1 µL of DMSO, 0.5 µL of 20 mM of GTP, 0.5 µL of 100 mM ATP, 0.5 µL of 20 mM $MgCl_2$ were combined and adjusted to a final volume of 10 µL with BRB-80. A second solution was created with the same contents, but 0.5 uL of 2 uM KSP-18 406 motors (kinesin-5) were also added to solution. These solutions were incubated in a 37°C water bath for 5 min and then diluted into a 200 µL volume of BRB-80 supplemented with 10 µM taxol.

3.1.2 Microscope-based Imaging Assay

Several standard solutions were created according to a protocol for Standard Motility Assays developed by the Howard Lab, and the protocol was modified most recently by David Arginteanu of the Hancock Lab in 2014 so that the directions were clearly written. The solutions that were made include a BRB80CS0.5 solution which contains 0.5 mg/mL casein in BRB-80 buffer. Additionally, a BRB80CA solution was made that contains 0.2 mg/mL casein and 1 mM MgATP in BRB-80. Two solutions of BRB80CT were made (one for each sample) that contained 0.2 mg/mL casein and 10 µM taxol in BRB-80 buffer. 85 µL of the BRB80CT solution was required to make the motility solution which contains 1 µL of 100 mM ATP, 1 µL of 2 M D-glucose, 1 µL of 2 mg/mL glucose oxidase, 1 µL of 0.8 mg/mL catalase, 0.5 µL of beta mercaptoethanol (BME), and 10 µL of the microtubules that were polymerized in 3.1.1.

To image the microtubules, flow cells were created by adhering double sided tape to a microscope slide, and then placing a #1.5 coverslip on top (Corning). 20 µL of the BRB80CS0.5

solution was flowed into the cell, followed by 20 µL of approximately 1 µM Rigor 980 kinesin-1 full length motors, and lastly was 20 µL of the motility solution just before imaging. Each solution had a 5 minute delay between injections. The flow cell was then imaged at 100x magnification using oil immersion with an Epifluorescent Upright Microscope (Nikon) with a 100W Hg arc lamp and a ANDOR iXon Ultra microscope camera was used to capture the images. MicroManager was the imaging software. The filter of the microscope was set for orange light which will reflect green so that the rhodamine microtubules can be seen. The gain of the system was set to 300 and the exposure time was adjusted to 100 ms. Images were captured and saved.

3.1.3 Quantifying Image Results

The images were counted by hand and the totals are summed up in a table in Excel. The mean and standard deviation of the totals were then calculated. The mean values of microtubule counts (per image) as a function of tubulin concentration were plotted using Excel and standard error bars were added to the figure.

3.1.4 Kinetics Experiments Using Plate Reader

The experiments performed in this section require the use of a special buffer which will be explained first. Next, the experimental for the results shown in Figure 3-5 will be given. The experiment tested the effect of Eg5 on microtubule nucleation and polymerization for a starting concentration of 20 µM. This experiment was performed with 10% (v/v) DMSO and 10 mM

ATP. Other experiments performed in this section are similar to the methods presented here but the setup was dependent upon the experimental conditions being tested.

The experimental buffer was created by adding 5000 µL of BRB-80, 100 µL of 20 mg/mL Casein, 100 µL of 0.1M $MgCl_2$, 100 µL of 0.2M P-Creatine kinase to help regenerate ATP, and 1 µL of b-mecaptoethanol to a 4699 µL solution of ddH_2O. The solution was vortexed and centrifuged before being aliquoted into 1.5 mL fractions.

The experimental solutions were created by using a 96 well reading plate (capacity volume of the wells were 350 µL). One well was filled with 90 µL of the buffer and 10 µL of DMSO. This well was used as the blank for the experiment. The well that did not contain Eg5 motors was created by adding 51 µL of the buffer to a separate well with 10 µL of DMSO, 4 µL of 25 mM GTP, 10 µL of 100 mM of ATP, 0.6 µL of 1.5 µg/mL of P-Creatine kinase, and 25 µL of 88 µM Cycled Tubulin was added at the very end just before imaging. The procedure for the well that added Eg5 motors was the exact same except only 41 µL of buffer was added and 10 µL of 1 µM Eg5 motors were added in its place. Again, the tubulin was added just before imaging.

The plate reader absorbance value was measured at 340 nm, the analysis length was 30 minutes, a measurement was taken every 20 seconds, and a total of 91 measurements were taken. Additionally, the plate was set to shake for 5 seconds before taking a measurement and to shake for 3 seconds between measurements to ensure sufficient mixing. All experiments were performed at 37°C.

3.1.5 Analysis of Kinetics Experiments

Raw data plots of absorbance as a function of time at 340 nm were created using MATLAB. Data were then corrected to show the difference between the maximum and minimum absorbance values for every trial completed in order to make the data comparable since not all experiments were run at the same time. These values were recorded and accumulated into a plot that compared the net absorbance value to the change in tubulin concentration. This plot was created in Excel and a linear regression line was fit between each pair of points that consisted of the same environmental conditions.

Additionally, a table was created to summarize all of the different conditions that were present in the different systems for each sample that was tested. The time to reach the half maximum value for each sample was also determined and recorded in this table.

3.2 Results

3.2.1 Microtubule Nucleation measured by Fluorescence Microscopy

The first set of experiment used fluorescence imaging to count the number of nucleated microtubules as a function of tubulin concentration and determine whether addition of kinesin-5 increased the rate of nucleation. Microscopy procedures were based on the gliding assay protocol that was developed in the Hancock Lab, but were modified in order to quantify the dependence of microtubule nucleation on tubulin concentration. For the microscope experiments, the free tubulin was allowed to incubate in a 37°C water bath for 5 minutes to allow nucleation to occur. Next, the microtubules were diluted into a taxol solution. The dilution

prevented further nucleation and growth, and the taxol stabilized any nucleated microtubules. To image the microtubules, a variation of the gliding assay (termed the Imaging Assay) was performed so that the microtubules would be attached to the surface of the coverslip by the full-length kinesin motors that were fixed into the flow cell. The nucleated microtubules are made from rhodamine-labeled tubulin which will fluoresce when the microtubules are imaged using green excitation. The combination of the fluorescent microtubules anchored to a 2-D surface creates a countable image of microtubules. Five images were recorded and the microtubules were counted and averaged. This procedure was performed for tubulin concentrations of 4, 6, 8, 10, and 15 µM, as shown in Figure 3-1.

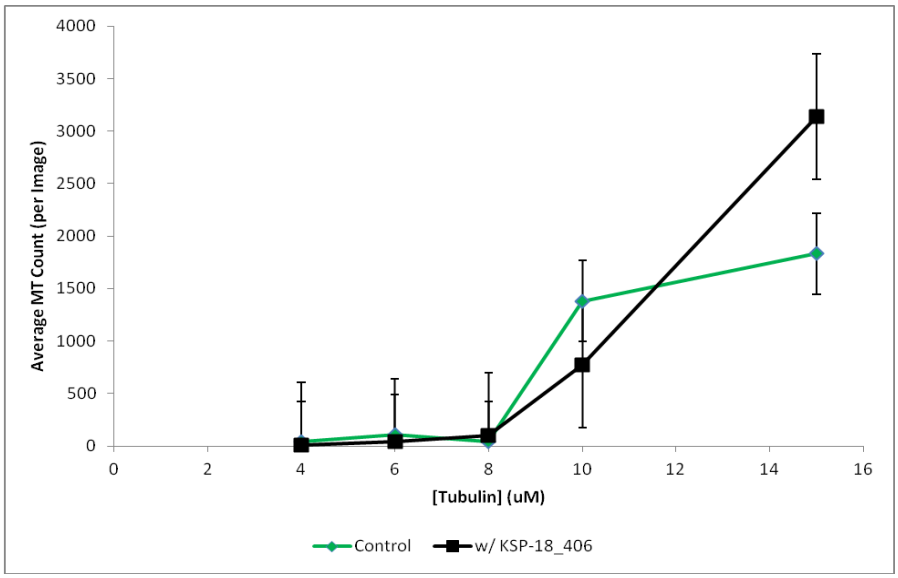

Figure 3-1. Microscope Experiment determination of Eg5 effect on nulceation. Average MT Count (per Image) vs. [Tubulin] from microscope experiments with standard error bars for N = 5 fields per tubulin concentration.

Figure 3-1 shows the effect of tubulin concentration on the nucleation of microtubules. It can be seen that at the lower concentrations of tubulin, there appears to be an unsubstantial

difference between the control and experimental groups. What can be inferred from this is that Eg5 has little or no effect on the nucleation rate at tubulin concentration levels below some minimum value. At the higher concentration levels, particularly at the 15 µM, the results do show a substantial difference between the control and experimental groups. These results suggest that at some concentration level between 10 and 15 µM, the effect of Eg5 may begin to increase the rate of nucleation in vitro while the rate of the control is unaffected.

3.2.2 Microtubule Nucleation Kinetics measured by Plate Reader

The plate reader experiments were performed as a supplement to the microscope experiments because the results can be used to help support the claims made about Eg5's effect on microtubule nucleation. Additionally, the kinetics data can be used to determine the critical concentration of tubulin at which nucleation will occur. For the kinetic experiments, several different conditions were tested on two different tubulin concentrations (10 and 20 uM) including DMSO, the addition of 100 nM Eg5 motors, and ATP. The complete list of parameters for every experiment is outlined in Table 3-1.

Table 3-1. Summary of experimental conditions for all kinetics experiments performed using the plate reader. The Figure Plotted column identifies where the absorbance plot for the given set of experimental conditions is located.

Conc. (uM)	Temp (°C)	DMSO	Eg5 (nM)	ATP (mM)	Volume (uL)	Figure Plotted
10	37	0	0	0	100	3-2
	37	10% vol.	0	0	100	3-3
	37	10% vol.	0	0	100	3-4
	37	10% vol.	100	0	100	3-4
	37	10% vol.	0	10	300	3-6
	37	10% vol.	100	10	300	3-6
20	37	0	0	0	100	3-2
	37	10% vol.	0	0	100	3-3
	37	10% vol.	0	0	100	3-4
	37	10% vol.	100	0	100	3-4
	37	10% vol.	0	10	100	3-5
	37	10% vol.	100	10	100	3-5

Figures 3-2 through 3-6 are plots of absorbance vs. time. The absorbance of the reactions was measured at 340 nm for 1800 seconds. Figure 3-2 plots the time response of 10 and 20 µM tubulin in the absence of DMSO, Eg5, and ATP. The $t_{1/2}$ Max for the 10 µM sample was 207 s and the $t_{1/2}$ Max for the 20 µM sample was 1330 s.

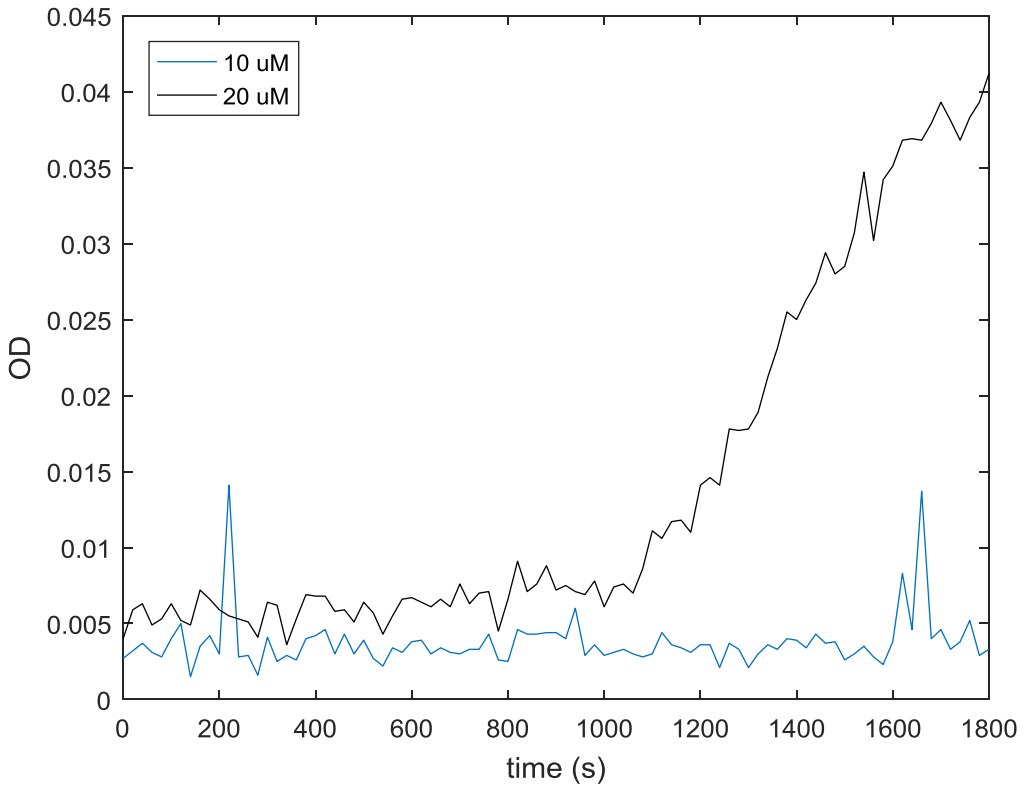

Figure 3-2. Microtubule nucleation kinetics experiment. Absorbance at 340 nm vs. time of microtubule nucleation in varying tubulin concentration (37ºC), also in the absence of DMSO, Eg5 motors, and ATP. The total volume of the solutions that were measured was 100 uL.

The absorbance responses for both signals in Figure 3-2 yielded low values (< 0.05 OD) which may reduce the signal to noise ratio. After the 1000 s time point, the absorbance for the 20 µM tubulin sample began to increase, indicating that some nucleation and polymerization occurred, but the 10 µM appeared to not increase with time. This lack of increase in absorbance suggests that nucleation does not occur or cannot be sustained at the in vitro conditions tested in this experiment.

In order to potentially induce nucleation, 10% (v/v) DMSO was added to the samples that were plotted in Figure 3-3. The figure shows the time response of 10 and 20 µM tubulin in the

presence of 10% (v/v) DMSO and in the absence of Eg5 and ATP. The $t_{1/2}$ max was 326 s for the 10 µM sample and 175 s for the 20 µM sample.

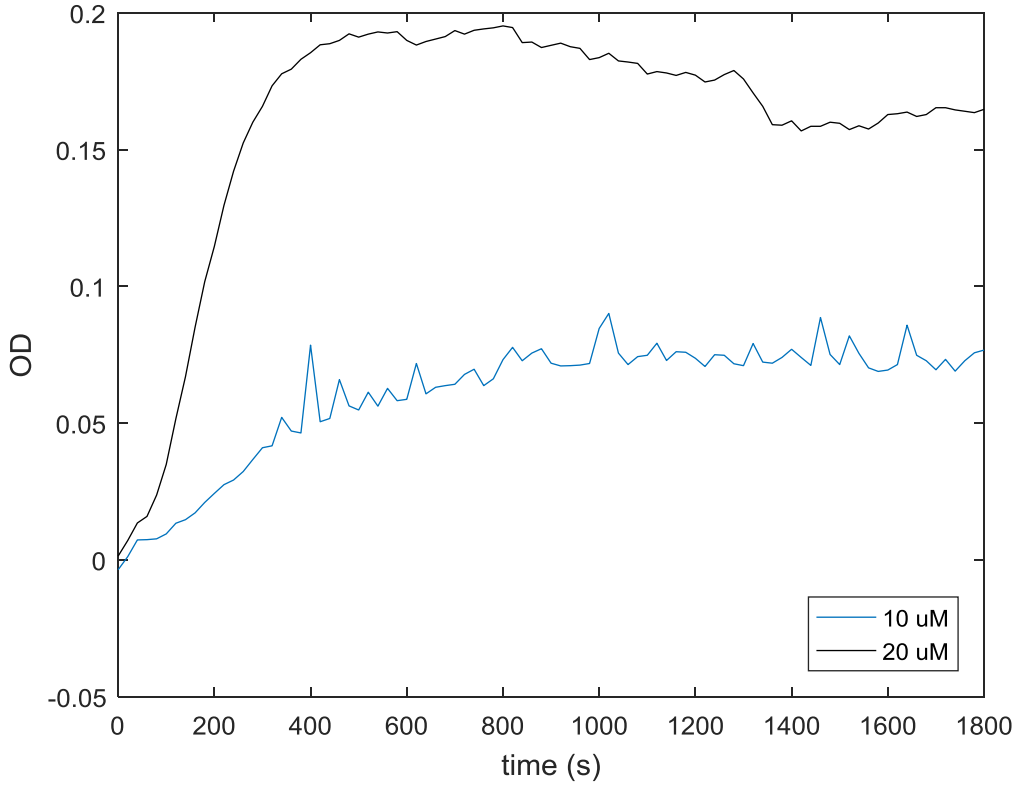

Figure 3-3. Microtubule nucleation kinetics in 10% (v/v) DMSO. Absorbance at 340 nm vs. time of microtubule nucleation in varying tubulin concentration (37ºC) in the presence of 10% (v/v) DMSO, but in the absence of Eg5 motors and ATP. The total volume of the solutions that were measured was 100 uL.

The addition of DMSO resulted in an increase in absorbance. The 10 µM sample still has some noise in the signal but the results are distinguishable because both samples show an apparent sigmoidal curve with a measurable absorbance. The sigmoidal curves suggest that DMSO is very important for the system because the sigmoidal growth curve is the natural shape of microtubule growth [cite]; therefore, if the absorbance was low in Figure 3-2 relative to Figure

3-3, the addition of DMSO had an effect that initiated the nucleation and polymerization of microtubules.

Next, the effect of Eg5 on microtubule nucleation was tested by repeating the experiment in Figure 3-3 but with the addition of Eg5 motors. Figure 3-4 plots the time response of 10 and 20 µM tubulin in 10% (v/v) DMSO but in the absence of ATP. The overall reaction volume was 100 µL. The $t_{1/2}$ max for the 10 µM sample without Eg5 was 346 s and the value for the 20 µM sample without Eg5 was 210 s. The $t_{1/2}$ max for the 10 µM sample with Eg5 was 510 s and the value for the 20 µM sample with Eg5 was 199 s.

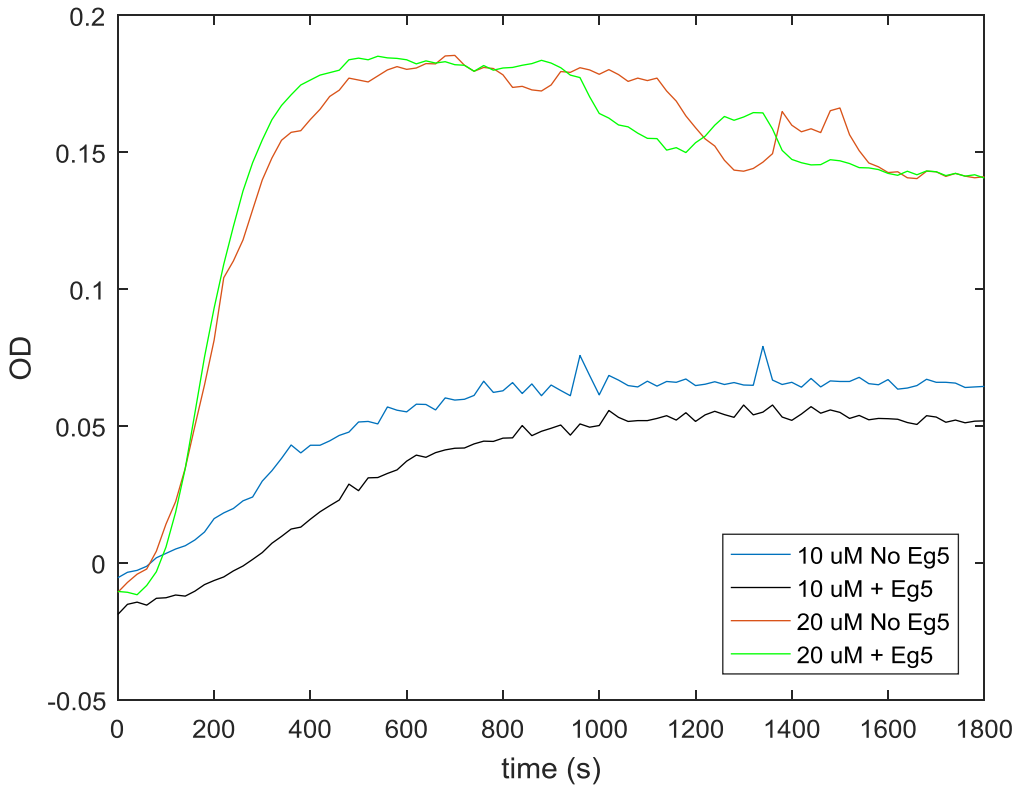

Figure 3-4. Microtubule nucleation kinetics as a function of Eg5. Absorbance at 340 nm vs. time of microtubule nucleation with changing conditions of both tubulin concentration and Eg5 motors [100 nM] (37ºC) in the presence of 10% DMSO by volume but in the absence of ATP. The total volume for the solutions that were measured was 100 uL.

The results in Figure 3-4 also show the sigmoidal relationship that was present in Figure 3-3. For the 20 µM samples, there is some noise present in the signals, but the results appear almost identical to each other which would suggest that Eg5 does not have an effect on microtubule nucleation. For the 10 µM samples, the addition of Eg5 actually reduced the maximum absorbance by a substantial amount. The difference in absorbance between the two signals becomes apparent when the $t_{1/2}$ max is compared. The sample without Eg5 motors reached its half maximum in 346 s while the Eg5 containing sample reached its half maximum within 510 s.

Because the results of Figure 3-4 yielded unexpected results, the experiment was repeated but ATP was added to allow Eg5 motors to processively walk on the microtubules, which enhances their ability to reach the microtubule plus-ends. Figure 3-5 plots the time response of 20 µM tubulin while comparing the effects of Eg5 in the presence of 10% (v/v) DMSO as well as ATP. The overall reaction volume was 100 µL. The $t_{1/2}$ max for the no Eg5 added sample was 246 s while the Eg5 added sample was 239 s.

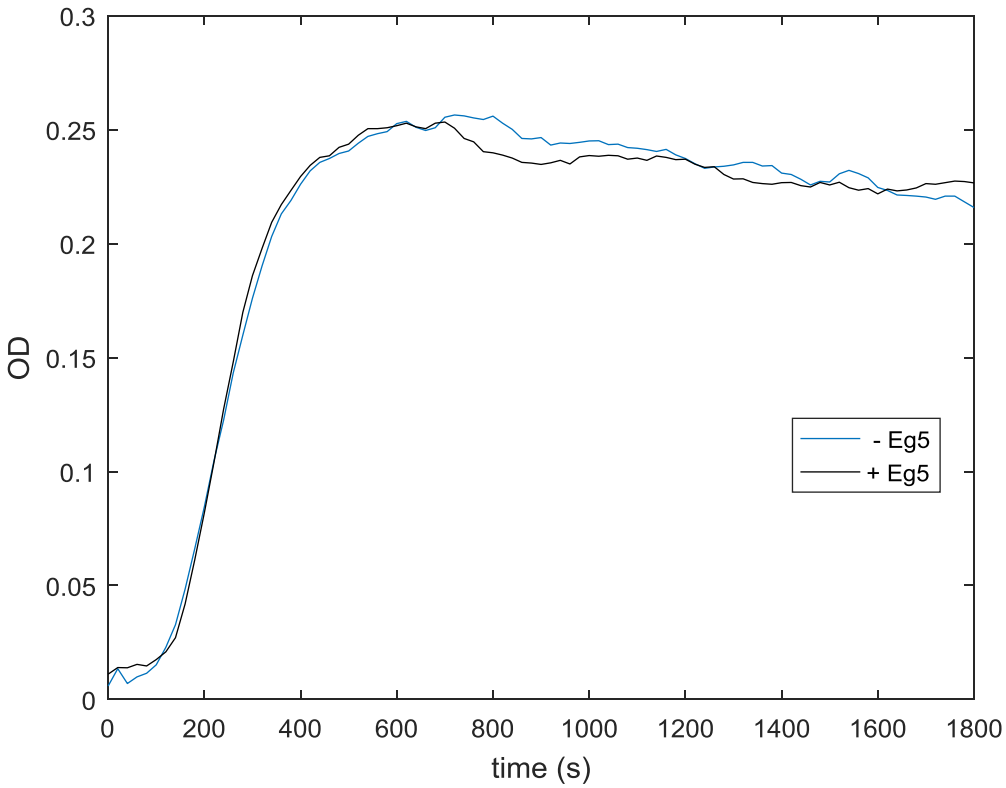

Figure 3-5. 20 µM Microtubule nucleation kinetics with ATP. Absorbance at 340 nm vs. time of microtubule nucleation with changing conditions of Eg5 motors [100 nM] (37ºC) in the presence of a 20 µM tubulin concentration, 10% DMSO by volume, and ATP. The total volume of the solutions that were measured was 100 µL.

The curves for Figure 3-5 virtually superimpose, which is also evidenced by the fact that their times to their half maximums differ by only 7 seconds (246 s for no Eg5 and 239 s for Eg5). Due to the addition of ATP, the absorbance increased; in Figure 3-4, the maximum absorbance did not exceed 0.2, but the value here is approximately 0.25, consistent with a final microtubule polymer level when ATP is present.

Figure 3-6 shows the same experimental design as Figure 3-5 except with 10 µM tubulin. The overall reaction volume was increased to 300 µL in order to reduce noise in the signal. The $t_{1/2}$ max for the no Eg5 sample was 114 s while for the Eg5 added sample it was 284 s.

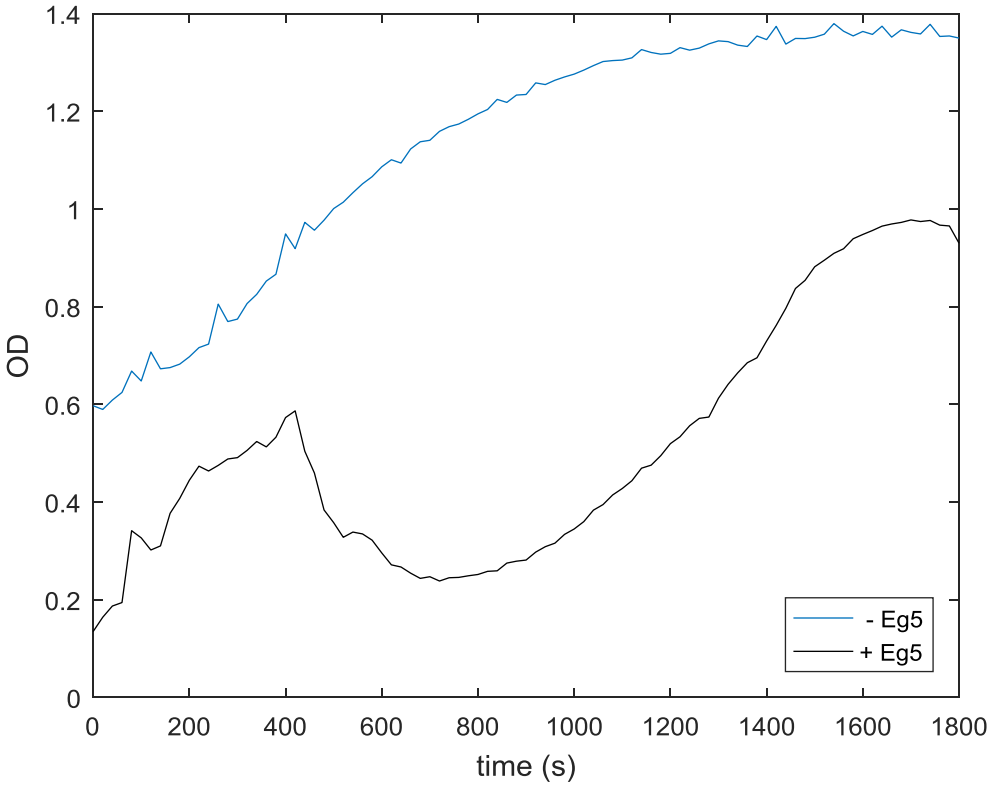

Figure 3-6. 10 µM Microtubule nucleation kinetics with ATP. Absorbance at 340 nm vs. time of microtubule nucleation with changing conditions of Eg5 motors [100 nM] (37ºC) in the presence of a 10 µM tubulin concentration, DMSO, and ATP but the reaction volume was expanded to 300 µL.

The reduction in noise in the signals is apparent from the plots in Figure 3-6; however, the absorbance values increased substantially. The absorbance increased more than 25 times above the maximum absorbance for the 100 µL samples. One unusual difference about these results is that the initial absorbance is not located at zero when time is zero. It is important to point out though that at the 10 µM concentration, there is a substantial difference in the half maximum values. The sample that did not have Eg5 reached its half maximum within 114 s while the added Eg5 sample progressed slower and reached its half maximum in 284 s.

Next, the net OD change was calculated for each sample (max - min) and these values were plotted in relation to their corresponding concentration of the same experimental conditions. The matched pairs of points were fitted to a linear regression line. Figure 3-7 shows the resulting plot for the linear regression fits and the legend provides the description of the experimental differences between each pair of points.

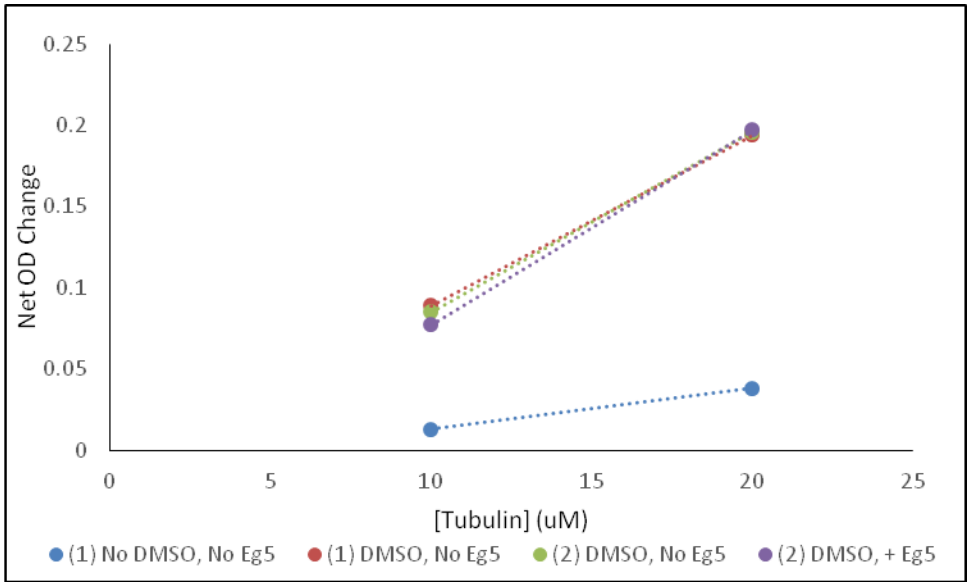

Figure 3-7. Net OD Change vs. [tubulin] for the various conditions tested in Figures 3-2 through 3-4. The Absorbance value measured during the experiments was 340 nm for 10 and 20 μM [Tubulin]. A linear regression was fitted to each pair of points for the same experimental conditions. The linear regression equations are given in Table 3-2. The points marked (1) were measured on a separate day from the points marked (2).

In addition to showing the net OD change for the different experiments tested using the plate reader, the $t_{1/2}$ max times for the same conditions were summarized into Figure 3-8 to show the change in the rate of polymerization as a function of tubulin concentration.

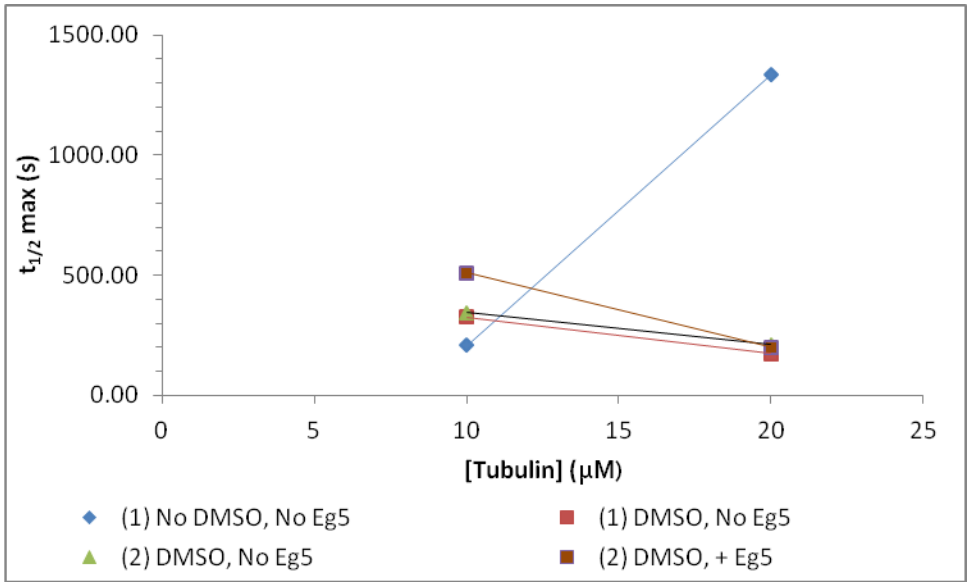

Figure 3-8. $t_{1/2}$ max times (s) vs. [Tubulin] for the various conditions tested in Figures 3-2 through 3-4. The $t_{1/2}$ max measurements for the different experiments performed. A linear regression was fitted to each pair of points to show the gradient of change in their values as a function of [tubulin].

The data in Figure 3-7 appear to overlap except for the line in which DMSO was not added to the solution. All of the net absorbance values were higher at the 20 µM concentration which is indicative that the rate of nucleation is dependent upon tubulin concentration. The equations for the linear regression lines are presented in Table 3-2. The linear regressions were used to calculate the critical tubulin concentration at which the net absorbance would yield a value of zero (y = 0). These values were also added to Table 3-2.

Table 3-2. Summary of linear regression equations that corresponds to the regression lines that were fitted in Figure 3-7. In addition to the linear regression equations, the critical tubulin concentration determined from each linear regression (substituted y = 0, solved for x) was calculated.

Tubulin Conditions	Linear Regression Equation	Critical Tubulin Conc. (µM)
(1) No DMSO, No Eg5	y = 0.0025x - 0.012	4.80
(1) DMSO, No Eg5	y = 0.0105x - 0.016	1.52
(2) DMSO, No Eg5	y = 0.0111x - 0.026	2.34
(2) DMSO, + Eg5	y = 0.0120x - 0.043	3.58

The average value for the calculated critical tubulin concentration is 3.06 µM. Relative to a similar experiment done by Wieczorek et al. (2015), the critical tubulin concentration was determined to be about 1 µM by their calculations. However, their experimental results showed no nucleation within the range of 1 to 6 µM. The results of this experiment are shown in Figure 3-9 [56].

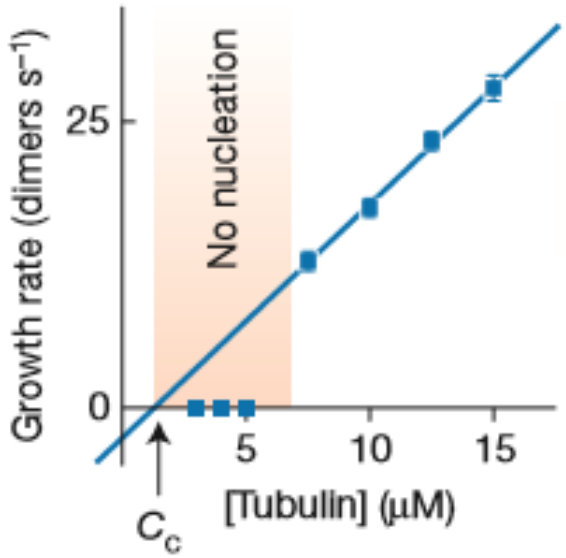

Figure 3-9. Determination of the critical tubulin concentration via linear regression. The results of the experiment determined that the critical tubulin concentration is about 1 µM. However, the experimental results showed no microtubule nucleation until a 6 µM of tubulin was added. Figure adapted from Wieczorek et al. (2015) [56].

3.3 Discussion

The experiments outlined above were carried out to determine whether Eg5 affected microtubule nucleation. It was previously shown that microtubule nucleation is dependent upon γ-TuRC and that kinesin-5 is a microtubule polymerase. Therefore, the prediction was that Eg5

should enhance microtubule nucleation. The results presented in Section 3.2 cumulatively provide an inconclusive answer to the question of whether Eg5 affects microtubule nucleation. The results presented in Section. 3.2.1 were modeled after a figure presented in a publication by Zheng et al. (1995), except the goal was to show a nucleation dependence on Eg5 instead of γ-TuRC. In Figure 3-1, the microtubule counts per image show no dependence on Eg5 at low tubulin concentrations (≤ 10 μM) because the difference in the counts per image is not substantially significant between the control and experimental groups. Figure 3-1 does show a substantial difference at the 15 μM tubulin because the number of microtubules per image in the experimental group was substantially higher than the control group. The results do not definitively demonstrate that Eg5 has a positive effect on the nucleation of microtubules because although the rate of nucleation increased for one tubulin concentration, more data points at higher tubulin concentrations would need to be added in order to substantiate that Eg5 induces an effect. More experiments would have to be conducted in order to definitively determine whether Eg5 induces microtubule polymerization.

The microtubule nucleation kinetics experiments were meant to supplement and support the findings of the results presented in Figure 3-1. The question to be answered is whether Eg5 effects the nucleation of microtubules. The process of microtubule nucleation is followed by polymerization but in the event that polymerization does not occur, the nucleus will degrade. Therefore, the prediction is that enhancing the polymerization of microtubules should increase the nucleation of more microtubules because more nuclei will be stabilized. Alternatively, Eg5 can enhance nucleation like a template similar to the model presented with γ-TuRC [40].

The results in Section 3.2.2 do not agree with the results of the microscope experiments. First, the kinetics experiments concluded that DMSO was an essential component of the in vitro

environment for microtubule nucleation. The dependence of DMSO was demonstrated through the results in Figures 3-2 and 3-3. The absorbance vs. time plot in Figure 3-2 showed very little absorbance, indicating a low rate of microtubule nucleation and polymerization, when compared to Figure 3-3 in which DMSO was added to the sample volumes. The absorbance plot in Figure 3-3 displayed sigmoidal curves which was indicative of microtubule nucleation and polymerization occurring because the rise in absorbance indicates that tubulin dimers are fusing together.

Additionally, the effect of Eg5 was experimentally tested to determine its effect on microtubule nucleation. The results in Figure 3-4 did not agree with the results in Figure 3-1. The curves in the figure show a sigmoidal shape which is similar to Figure 3-3 and so it is inferred that nucleation and polymerization of microtubules is occurring. However, the results of the 10 µM tubulin show a decrease in absorbance for the sample containing Eg5 relative to the control. The 20 µM tubulin samples show a nearly identical absorbance for all time points between the experimental and control groups. The $t_{1/2}$ maximum value that defines the time at which the sample has reached its half maximum absorbance can help distinguish differences between how fast the absorbance rates are increasing. For Figure 3-3, the $t_{1/2}$ max for the 10 µM was 326 s and the $t_{1/2}$ max for 20 µM was 175 s. It can be inferred from these values that the 20 µM is increasing absorbance at a faster rate than 10 µM. This value makes sense because more tubulin in the sample should yield a higher rate of nucleation and polymerization of microtubules. Therefore, if the $t_{1/2}$ maximums were to be analyzed for the samples in Figure 3-4, a positive effect on the rate of nucleation would result in a faster $t_{1/2}$ max relative to the control. A negative effect on the rate of nucleation would result in a slow $t_{1/2}$ max relative to the control, and no effect by Eg5 would yield no change in the $t_{1/2}$ maximum value. The foundation for this

concept is derived from the proposed mechanism of Eg5 acting as a microtubule polymerase [5]. In the work by Y. Chen and Hancock, Kinesin-5 increases the rate of polymerization while interpreting that this is done by stabilizing newly bound protofilaments on the plus end of a microtubule. Another positive effect of Eg5 acting as a polymerase is that the rate of catastrophe is decreased if Eg5 is bound to the microtubule surface during polymerization [5]. Therefore, the same concepts should apply here. The $t_{1/2}$ max for the 10 µM samples in Figure 3-4 were 346 s (Control) and 510 s (Eg5). The $t_{1/2}$ max for the 20 µM samples were 210 s (Control) and 199 s (Eg5). The times for the 10 µM samples show a substantial increase between the control and the experimental which is indicative of a negative effect of Eg5 on microtubule nucleation. The 20 µM samples show a very small difference in absorbance change which is interpreted as no change. Eg5 yields no effect on microtubule nucleation in the higher concentration samples which is a direct contradiction with the results reported in Figure 3-1.

Figure 3-5 and 3-6 re-evaluated the experimental conditions tested in Figure 3-4 but in the presence of ATP. The results were consistent with what was found in Figure 3-4. In Figure 3-5 (20 µM samples), the curves show nearly identical sigmoidal relationships. The $t_{1/2}$ maximums for the samples were 246 s (Control) and 239 s (Eg5). Values that are too similar to be treated as different and support the notion that Eg5 does not affect microtubule nucleation. Figure 3-6 shows very abnormal plots because the volume of the samples was increased to 300 µL to help reduce noise in the signal, but this increase in volume may have caused solution to spill out of the well during mixing. The experimental group yielded an overall absorbance that was lower than the control group and the $t_{1/2}$ max values were 114 s (Control) and 284 s (Eg5). Again, the results support the findings in Figure 3-4 that at a lower tubulin concentration of 10 µM, Eg5 has a negative effect on microtubule nucleation. These results are a contradiction to the

results reported above in which Figure 3-1 displayed evidence that Eg5 positively effects microtubule nucleation.

Figure 3-7 shows the linear relationship between the net absorbance change and tubulin concentration. The figure showed that for all of the conditions in which DMSO was added, the net absorbance values did not change substantially based on tubulin concentration. Because the net absorbance did not change substantially regardless of the conditions, this is another piece of evidence in support for the claim that Eg5 does not affect microtubule nucleation.

From the linear regressions plotted in Figure 3-7, the critical concentration of microtubule nucleation can be quantitatively determined. The summary of these results was given in Table 3-2. Each linear regression was solved to determine a critical tubulin concentration in which nucleation would not occur. Effectively, the value of the absorbance change would be 0. The critical tubulin concentrations calculated from the linear regressions were averaged to determine a consistent critical concentration. The value averaged to be 3.06 μM. A similar analysis was done in a publication by Wieczorek et al. (2015) in which they measured microtubule growth rates as a function of tubulin concentration. Their findings upon extrapolating their fitted linear regression were that the critical concentration for nucleation was found at 1.3 μM but their experimental results showed no nucleation in the tubulin range of 1-6 μM [56]. Therefore, the results reported in Figure 3-7 and Table 3-2 correspond to the findings of Wieczorek et al. (2015) in Figure 3-9.

The results shown in Figure 3-8 provide evidence that microtubule nucleation and polymerization is a function of [tubulin]. Aside from the No DMSO, No Eg5 conditions, the other experiments showed a decrease in $t_{1/2}$ max time which is indicative that the rate of increase in absorbance is faster for the higher concentrations of tubulin.

In addition to reporting the results presented here, some insight will be provided into the potential findings of experiments involving Kinesin-5 inhibitors. Based on the work presented by Chen et al. (2017), Eg5 inhibitors can be classified into two classes, weak- or strong- binding. If these two kinds of inhibitors were to be introduced into the experiments presented above, the results should not remain constant. For the weak binding-inhibitors, it would be expected that the sigmoidal nucleation/polymerization curve would shift rightward compared to just Eg5. This is because weak-binding inhibitors do not allow Eg5 to bind tightly to the microtubule. Even though a bound motor would be very processive, which would create stabilization of added protofilaments and increase microtubule length, but the motor is also more likely to unbind form the microtubule due to a weak tethering. Therefore, the weak-binding inhibitors would be able to continually bind, dissociate, and bind to the same or a new microtubule and cause the amplification of nucleation. In contrast, the strong-binding inhibitors would shift the nucleation/polymerization curve leftward. It would be shifted leftward because strong-binding inhibitors cause Eg5 to anchor to microtubules tightly. This tight binding causes them to not be processive and does not allow them to detach very often. If a Kinesin-5 motor binds to a microtubule indefinitely, shouldn't this provide much stabilization for the binding protofilaments? Yes, it should, but this would only be effective if the motor was bound at the edge of the plus end. In Y. Chen and Hancock's proposed model for a Kinesin-5 polymerase, one of the key foundations of the microtubule stabilization was the fact that the motor stepped before the recently added protofilament detached. Therefore, if the motor is not processive, it should not increase nucleation very much. The added benefit of using strong-binding inhibitors is that the microtubule will not degrade. This was effectively shown in the introduction (Section

1.2.3) in which the microtubule shrinkage rate for a strong-binding inhibitor was essentially 0 nm/s. The figure that supports this notion was adapted from Chen et al. (2017).

Therefore, the results of the nucleation experiments yielded inconclusive results. The next step would be to replicate the experiments to recreate the results so that the data presented can be supported or refuted. To the best of the author's knowledge, this is the only known work that examines the effect of Eg5 on microtubule nucleation.

Chapter 4

Conclusion

The synthesis, purification, and characterization procedures presented in this thesis provide a workable protocol for definitively synthesizing mant-labeled adenosine triphosphate (mATP). The results presented on the different characterization methods (UV-VIS, Fluorescence, Kinetics) are consistent with the values reported in literature. The use of these fluorescent nucleotides provides a method for quantifying on- and off- rates in nucleotide binding for different kinesin variants.

This thesis also shows that the experiments conducted to investigate the effect of Eg5 on microtubule nucleation is inconclusive. The results of the microscope experiments definitively showed that Eg5 has a positive effect on microtubule nucleation at concentrations of tubulin higher than 10 µM, but the nucleation kinetics experiments showed opposite results. At a concentration of 10 µM, Eg5 was shown to have a negative effect on microtubule nucleation and no effect at a concentration of 20 µM. The averaged critical concentration for no nucleation in vitro is 2.48 µM. More experiments and replication of results are needed in order to support or refute the claims presented in this thesis.

Appendix A:

Standard Operating Procedure for Synthesizing, Purifying, and Characterizing mant-labeled Adenosine Triphosphate (mATP)

The Pennsylvania State University
Department of Biomedical Engineering
Hancock Lab: Molecular Biomechanics
Written by: Colin Lingafelt

Summary

This Standard Operating Procedure outlines the processes necessary in order to synthesize, purify, and characterize mant-labeled nucleotides. The synthesis reactions involve strict pH balance as well as an incubation time of approximately 2 hours. The products can then be purified via Anion Exchange Column (DEAE-Sephadex) in a linear gradient buffer (Triethylammonium bicarbonate 5mM to 900 mM). Characterization of the products is determined in the three following ways. First, the Absorbance Spectrum (UV-VIS) relative to known mant-labeled derivatives was used as a benchmark for concentration of samples. Next, Fluorescence data of mant-labeled derivatives in solution was obtained using a fluorimeter. This data was then tested against a solution containing molecular motors (KIF3A). An increase in the fluorescence was regarded as wanted products based on the results of other literature. Finally, kinetic data can be determined by manually computing on-/off- rates for the mant-labeled nucleotides when added to a solution of molecular motors (KIF3A). This solution was then flushed out with a saturated amount of ATP. After the data was collected, the rates were determined, using MATLAB, by fitting a single exponential to the data curves. The coefficients were then cross-referenced with other literature for validity. The products obtained with these procedures are capable of being used in other experiments and preps in the laboratory.

Synthesis procedure

1. Dissolve 10 mmol of nucleotide in 15 mL of water in a 125-mL Erlenmeyer flask.

2. Add 15 mmol of methylisatoic anhydride to the solution.

3. Adjust pH to 9.6 using 2N/2M NaOH.

4. Place into incubator at 37 degrees Celsius for 2 hours and shake at 250 rpm.

   - Check pH using pH strips every 20 minutes, adjust pH by adding more NaOH if necessary.

5. After the reaction is completed, allow mixture to cool and then change the pH to 7.0 by adding 1N/1M HCl as needed.

- Use pH strips to check.

6. Place mixture into a 50-mL bottle with a screw cap and place into the freezer overnight.

Purification procedure

1. Remove sample and allow to thaw.

2. Turn lamp on and check to make sure that the DEAE FF column is correctly attached to the FPLC.

3. Prepare 2 Triethylammonium Bicarbonate (TEAB) buffer solutions from the following:

- Need one solution at 5 mM TEAB and one 900 mM TEAB

- A linear gradient is needed to elute sample from the column, this will be created
by mixing the solutions of 5 mM and 900 mM in the FPLC system

- Make sure there is at least 250 mL of each buffer.

- Check pH of buffers, pH 8.5 is required, add HCl if necessary.

4. Place both buffer solutions on ice and degas until the column is ready to be executed.

5. Load procedure onto the computer "IExDEAE5mL 2mL sample" which is located under the Ion Exchange folder.

- DO NOT PRESS "RUN" UNTIL BUFFER IS LOADED INTO PUMP SYSTEM

6. Once the sample is thawed, use a 3 mL syringe and needle to extract 2 mL of the sample.

- Remove the air bubbles and decrease the volume of the syringe to 1.5 mL, add red injector tip to the end of syringe.

7. Place buffers into FPLC. Low concentration (5 mM) goes into Pump A and High concentration (900 mM) goes into Pump B.

8. Take sample and screw into injection valve at proper insert, but do not inject sample into the column yet!

9. Press "Run" and follow the instructions on the screen, but be sure to place collection tubes into the elution grid.

- Samples 1-15 run left to right, Samples 16-30 run right to left in the second row, and so on... 56 are needed in total.

10. Take ethanol flasks and degas them while the column is running.

11. After the column is completed, be sure to TURN THE LAMP OFF, remove/dispose of syringe, store away any extra buffer, collect samples, and make sure that the lamp is turned off!!!

Analysis procedure

1. Check chromatogram from DEAE column, there should be 3 absorbance peaks (See Figure 1).

- If there are 3 distinct peaks, Peak #3 is of primary concern.

- If there are only 2 peaks, either the reaction did not occur, the reaction went to completion, or the column was saturated.

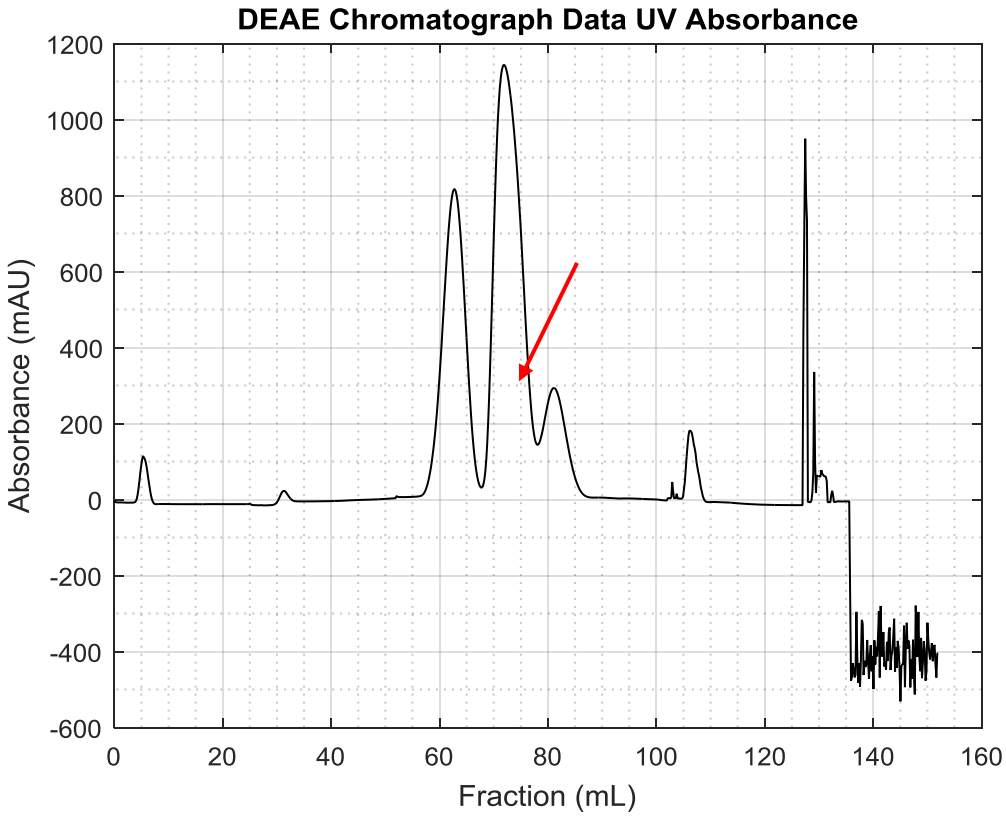

Figure 1: *This is a MATLAB representation of a mant-labeled nucleotide Chromatograph from the Unicorn system. As the column runs, it takes UV Absorbance data at a wavelength of 280 nm. If the reaction proceeds, the chromatograph of the column purification should look similar to this. Observe the location of the peak that the red arrow is pointing to. If this absorbance peak is present, then the sample collected in these corresponding fractions will contain your product for analysis.*

2. Correlate the sample numbers with the fraction elution volumes to determine which samples contain which peaks.

3. Test the absorbance of Peak #3 vs. store-bought mant-labeled nucleotide (See Figure 2).

- Store-bought mATP has an absorbance of 0.60 at 250 nm at a concentration of 25 uM. (ADD its absorbance at 356 nm)

- Dilute as needed to nearly match the absorbance, and compare ratio of peaks from 250 nm and 356 nm.

** A250/A356 should be > 3.50, this will also help to quantify the concentration of the sample. **

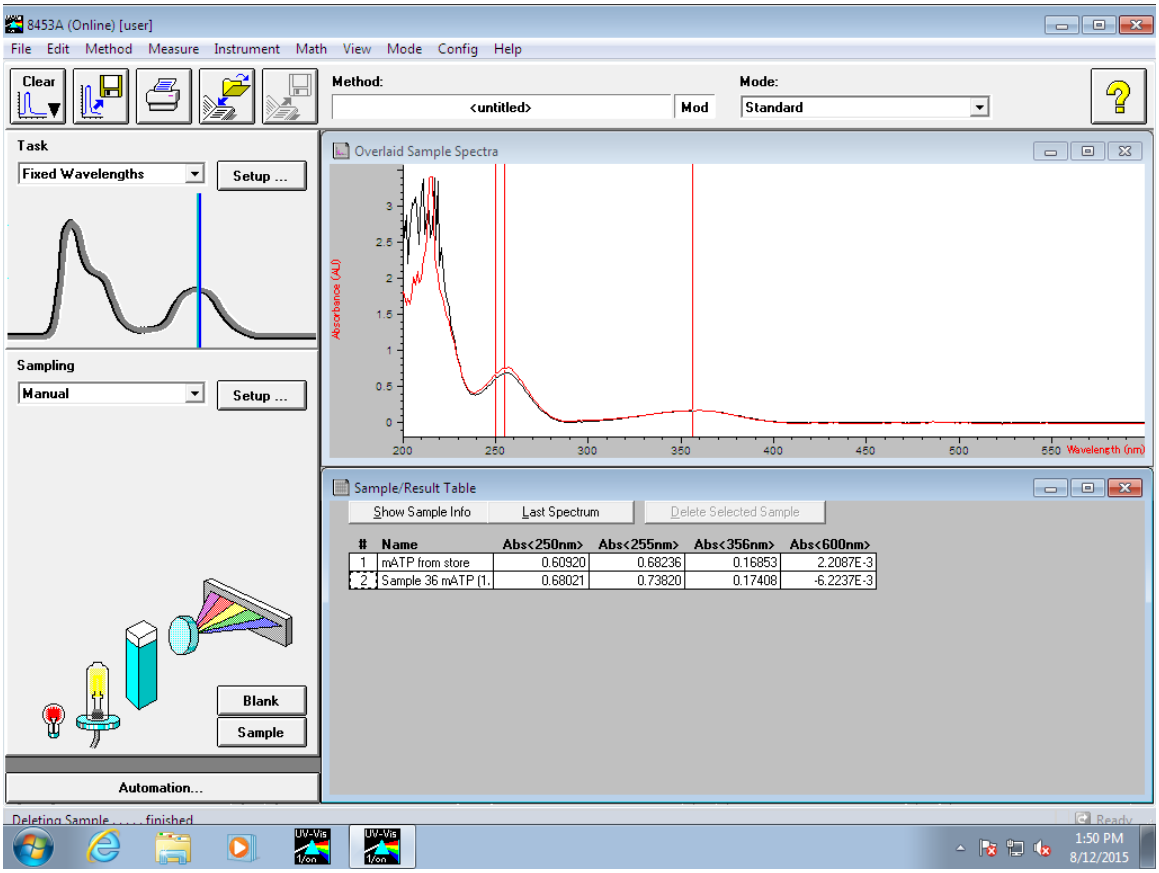

Figure 2: *Spectrophotometer data of store-bought mantATP vs. synthesized mantATP. Aliquots of store-bought mATP are found in concentrations of 100 uM. Sample was diluted to ¼ the concentration and the Absorbance of the sample was taken at 250, 255, and 356 nm (black curve). Knowing that the concentration should be around 25 uM, Beer's Law (A = εb[c]), where A is the absorbance of the sample, ε is the molar extinction coefficient, b is the slit width of the cuvette (1 cm), and c is the concentration of the sample, was used to determine the relative concentration of the sample. The synthesized sample was then diluted and the absorbance was taken (red curve) until the spectrums of the 2 samples matched as shown above. The relative concentration of the sample then determined the stock concentration of the solution.*

4. Test the fluorescence of the sample by adding KIF3A (Kinesin-2) motors to solution with mant-labeled nucleotide (See Figure 3).

- Have the spectrum emission scan from 400 nm to 500 nm, and have the excitation wavelength be 356 nm.

- In a buffer of BRB-80, there should be a peak fluorescence at 448 nm. (If you are working with a GFP protein there will be another peak around 510 nm from the GFP.)

- There should be a significant increase in the fluorescence of the solution after the motors have been added to solution.

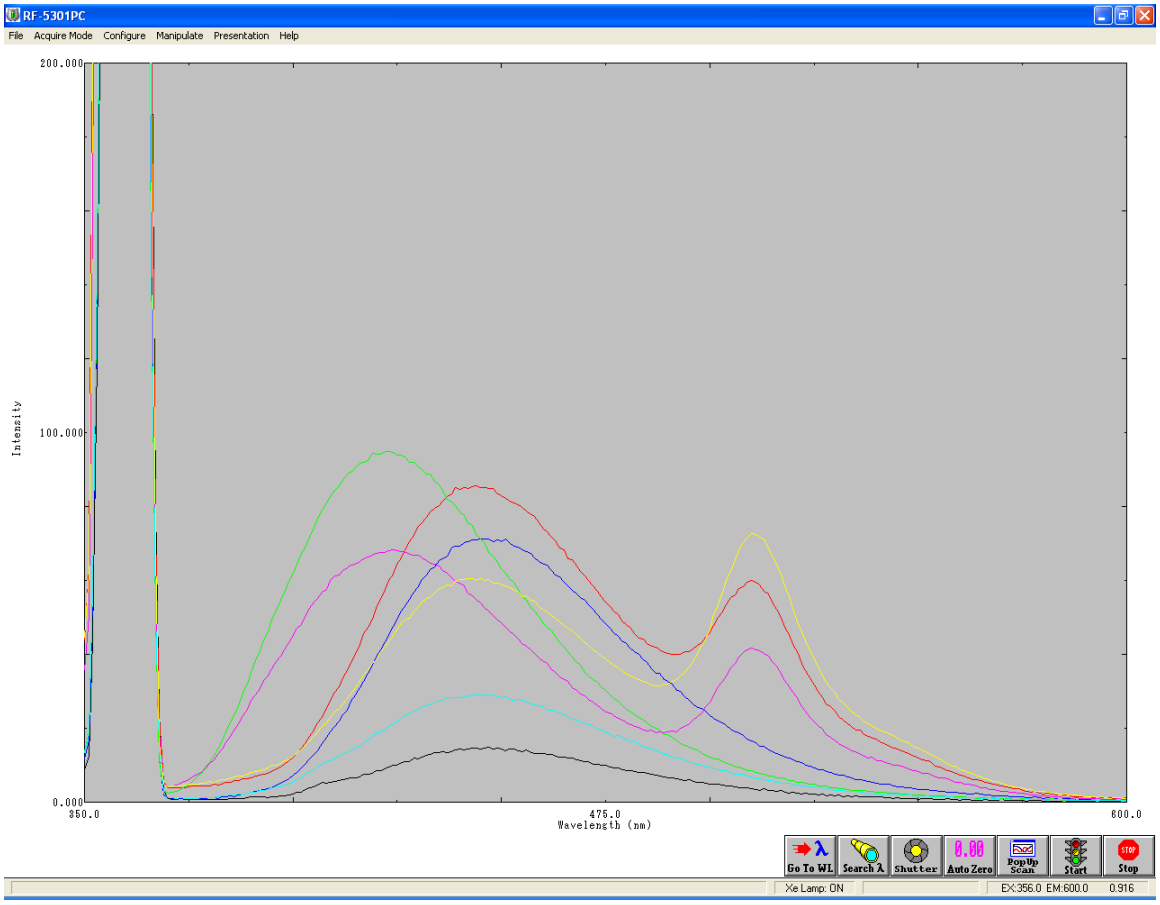

Figure 3: *Fluorimeter data of store-bought mant-labeled ATP vs. synthesized mantATP. The blue curve is the mant-labeled ATP that was store-bought and after adding KIF3A560GFP motors in BRB-80 the fluorescence increased as shown by the red curve. The same procedure was done with the synthesized mantATP and the teal curve is the fluorescence of the nucleotide alone. The same motors were added to solution and the yellow curve represents the change in fluorescence. The increase is much higher than the store-bought sample. The green and purple peaks are examples of products that are NOT mant-labeled ATP.*

5. Test the kinetics of the sample by using the kinetics mode of the fluorimeter and/or stopped-flow (See Figure 4).

- Use appropriate concentrations of motors (3A) and excess values of ATP

- The curves from this data can be fit to single exponentials to determine their goodness of fit based on literature reported values

- On-rate should be in the range 0.01-0.03 s^{-1}

- Off-rate should be in the range 0.001-0.002 s^{-1}

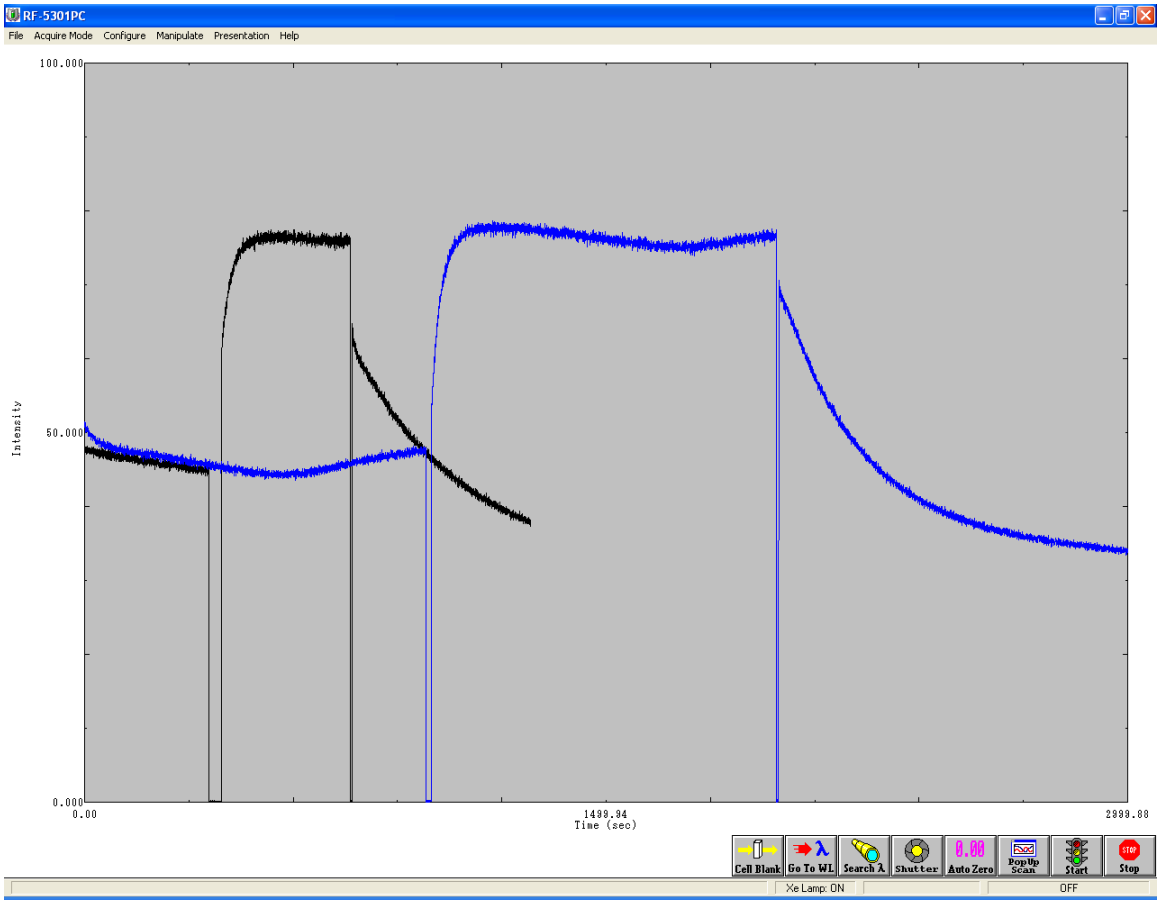

Figure 4: *Kinetics data on the fluorimeter was tested for store-bought mant-labeled ATP vs. the synthesized material. The black curve represents a test to observe the kinetics of the store-bought mantATP and to obtain a baseline for how the curve should look. The blue curve is the synthesized mantATP. It was the same experiment, the reaction was just carried out over a period of 3000 seconds. The exponential growth and decay curves can further be analyzed to determine an on- and off- rate for the mant-labeled nucleotides.*

REFERENCES

[1] T. Hiratsuka, "New ribose-modified fluorescent analogs of adenine and guanine nucleotides available as subtrates for various enzymes," *Biochim. Biophys. Acta (BBA)/Protein Struct. Mol.*, vol. 742, no. 3, pp. 496–508, 1983.

[2] Q. Ni, J. Shaffer, and J. a Adams, "Insights into nucleotide binding in protein kinase A using fluorescent adenosine derivatives.," *Protein Sci.*, vol. 9, no. 9, pp. 1818–27, 2000.

[3] G.-Y. Chen *et al.*, "Eg5 Inhibitors Have Contrasting Effects on Microtubule Stability and Metaphase Spindle Integrity," *ACS Chem. Biol.*, p. acschembio.6b01040, 2017.

[4] Y. Zheng, M. L. Wong, B. Alberts, and T. Mitchison, "Nucleation of microtubule assembly by a γ-tubulin-containing ring complex," *Nature*, vol. 378, no. 07 December 1995, pp. 578–583, 1995.

[5] Y. Chen and W. O. Hancock, "Kinesin-5 is a microtubule polymerase.," *Nat. Commun.*, vol. 6, p. 8160, 2015.

[6] S. M. Block, L. S. Goldstein, and B. J. Schnapp, "Bead movement by single kinesin molecules studied with optical tweezers.," *Nature*, vol. 348, no. 6299, pp. 348–52, 1990.

[7] R. D. Vale, T. S. Reese, and M. P. Sheetz, "Identification of a novel force-generating protein, kinesin, involved in microtubule-based motility.," *Cell*, vol. 42, no. 1, pp. 39–50, 1985.

[8] F. Kozielski *et al.*, "The crystal structure of dimeric kinesin and implications for microtubule-dependent motility," *Cell*, vol. 91, no. 7, pp. 985–994, 1997.

[9] E. Mandelkow and E. M. Mandelkow, "Kinesin motors and disease," *Trends Cell Biol.*, vol. 12, no. 12, pp. 585–591, 2002.

[10] N. Hirokawa, S. Niwa, and Y. Tanaka, "Molecular motors in neurons: Transport mechanisms and roles in brain function, development, and disease," *Neuron*, vol. 68, no. 4, pp. 610–638, 2010.

[11] H. Aizawa, Y. Sekine, R. Takemura, Z. Zhang, and M. Nangaku, "Kinesin Family in Murine

Central Nervous System," vol. 119, no. 5, pp. 1287–1296, 1992.

[12] D. H. Hall and E. M. Hedgecock, "Kinesin-related gene unc-104 is required for axonal transport of synaptic vesicles in C. elegans," *Cell*, vol. 65, no. 5, pp. 837–847, 1991.

[13] Y. Okada, H. Yamazaki, Y. Sekine-Aizawa, and N. Hirokawa, "The neuron-specific kinesin superfamily protein KIF1A is a uniqye monomeric motor for anterograde axonal transport of synaptic vesicle precursors," *Cell*, vol. 81, no. 5, pp. 769–780, 1995.

[14] C. Zhao *et al.*, "Charcot-Marie-Tooth disease type 2A caused by mutation in a microtubule motor KIF1Bbeta.," *Cell*, vol. 105, no. 5, pp. 587–97, 2001.

[15] N. Hirokawa, K. K. Pfister, H. Yorifuji, M. C. Wagner, S. T. Brady, and G. S. Bloom, "Submolecular domains of bovine brain kinesin identified by electron microscopy and monoclonal antibody decoration," *Cell*, vol. 56, no. 5, pp. 867–878, 1989.

[16] N. Hirokawa, Y. Noda, Y. Tanaka, and S. Niwa, "Kinesin superfamily motor proteins and intracellular transport.," *Nat. Rev. Mol. Cell Biol.*, vol. 10, no. 10, pp. 682–96, 2009.

[17] D. G. Cole, D. R. Diener, A. L. Himelblau, P. L. Beech, J. C. Fuster, and J. L. Rosenbaum, "Chlamydomonas kinesin-II-dependent intraflagellar transport (IFT): IFT particles contain proteins required for ciliary assembly in Caenorhabditis elegans sensory neurons," *J. Cell Biol.*, vol. 141, no. 4, pp. 993–1008, 1998.

[18] G. Ou, O. E. Blacque, J. J. Snow, M. R. Leroux, and J. M. Scholey, "Functional coordination of intraflagellar transport motors.," *Nature*, vol. 436, no. 7050, pp. 583–587, 2005.

[19] K. E. Sawin, K. LeGuellec, M. Philippe, and T. J. Mitchison, "Mitotic spindle organization by a plus-end-directed microtubule motor.," *Nature*, vol. 359, no. 6395, pp. 540–3, 1992.

[20] L. C. Kapitein, E. J. G. Peterman, B. H. Kwok, J. H. Kim, T. M. Kapoor, and C. F. Schmidt, "The bipolar mitotic kinesin Eg5 moves on both microtubules that it crosslinks," *Nature*, vol. 435, no. 7038, pp. 114–118, 2005.

[21] A. M. Saunders, J. Powers, S. Strome, and W. M. Saxton, "Kinesin-5 acts as a brake in anaphase

spindle elongation," *Curr. Biol.*, vol. 17, no. 12, pp. 453–454, 2007.

[22] K. Svoboda, C. F. Schmidt, B. J. Schnapp, and S. M. Block, "Direct Observation of Kinesin Stepping by Optical Trapping Interferometry," *NatureNature*, vol. 365, no. 6448, pp. 721–727, 1993.

[23] M. J. Schnitzer and S. M. Block, "Kinesin hydrolyses one ATP per 8-nm step.," *Nature*, vol. 388, no. 6640, pp. 386–90, 1997.

[24] D. L. Coy, M. Wagenbach, and J. Howard, "Kinesin takes one 8-nm step for each ATP that it hydrolyzes," *J. Biol. Chem.*, vol. 274, no. 6, pp. 3667–3671, 1999.

[25] M. L. Kutys, J. Fricks, and W. O. Hancock, "Monte carlo analysis of neck linker extension in kinesin molecular motors," *PLoS Comput. Biol.*, vol. 6, no. 11, 2010.

[26] W. O. Hancock, "The Kinesin-1 Chemomechanical Cycle: Stepping Toward a Consensus," *Biophys. J.*, vol. 110, no. 6, pp. 1216–1225, 2016.

[27] J. Q. Cheng, W. Jiang, and D. D. Hackney, "Interaction of mant-adenosine nucleotides and magnesium with kinesin," *Biochemistry*, vol. 37, no. 15, pp. 5288–5295, 1998.

[28] G. Y. Chen, D. F. J. Arginteanu, and W. O. Hancock, "Processivity of the Kinesin-2 KIF3A results from rear head gating and not front head gating," *J. Biol. Chem.*, vol. 290, no. 16, pp. 10274–10294, 2015.

[29] J. T. Patel, H. R. Belsham, A. J. Rathbone, and C. T. Friel, "Use of stopped-flow fluorescence and labeled nucleotides to analyze the ATP turnover cycle of kinesins.," *J. Vis. Exp.*, no. 92, p. e52142, 2014.

[30] R. C. Weisenberg, "Microtubule Formation in vitro in Solutions Containing Low Calcium Concentrations Author (s): Richard C . Weisenberg Published by : American Association for the Advancement of Science Stable URL : http://www.jstor.org/stable/1734230 JSTOR is a not-for-p," vol. 177, no. 4054, pp. 1104–1105, 1972.

[31] E. Mandelkow and E. M. Mandelkow, "Microtubules and microtubule-associated proteins," *Curr.*

Opin. Cell Biol., vol. 7, no. 1, pp. 72–81, 1995.

[32] J. Bryan and L. Wilson, “Are cytoplasmic microtubules heteropolymers?,” *Proc. Natl. Acad. Sci. U. S. A.*, vol. 68, no. 8, pp. 1762–6, 1971.

[33] W. a Voter and H. P. Erickson, “The Kinetics of Microtubule Assembly,” *Biol. Chem.*, vol. 259, no. 16, pp. 10430–10438, 1984.

[34] M. Srayko, A. Kaya, J. Stamford, and A. A. Hyman, “Identification and characterization of factors required for microtubule growth and nucleation in the early C. elegans embryo,” *Dev. Cell*, vol. 9, no. 2, pp. 223–236, 2005.

[35] J. J. Lindeboom *et al.*, “A mechanism for reorientation of cortical microtubule arrays driven by microtubule severing.,” *Science (80-.).*, vol. 342, no. December, p. 1245533, 2013.

[36] J. M. Kollman, J. K. Polka, A. Zelter, T. N. Davis, and D. A. Agard, “Microtubule nucleating γ-TuSC assembles structures with 13-fold microtubule-like symmetry,” *Nature*, vol. 466, no. 7308, pp. 879–882, 2010.

[37] J. M. Kollman, A. Merdes, L. Mourey, and D. A. Agard, “Microtubule nucleation by γ-tubulin complexes.,” *Nat. Rev. Mol. Cell Biol.*, vol. 12, no. 11, pp. 709–21, 2011.

[38] E. Nogales, M. Whittaker, R. A. Milligan, and K. H. Downing, “High-resolution model of the microtubule,” *Cell*, vol. 96, no. 1, pp. 79–88, 1999.

[39] E. Nogales, S. G. Wolf, and K. H. Downing, “Electron Crystallography,” *Nature*, vol. 391, no. January, pp. 199–204, 1998.

[40] D. Job, O. Valiron, and B. Oakley, “Microtubule nucleation,” *Curr. Opin. Cell Biol.*, vol. 15, no. 1, pp. 111–117, 2002.

[41] W. O. Hancock, “Aging Gracefully: A New Model of Microtubule Growth and Catastrophe,” *Biophys. J.*, vol. 109, no. 12, pp. 2449–2451, 2015.

[42] H. Lodish, *Molecular Cell Biology*, 4th ed. New York, NY: W.H. Freeman, 2000.

[43] K. J. Mickolajczyk, N. C. Deffenbaugh, J. Ortega Arroyo, J. Andrecka, P. Kukura, and W. O.

Hancock, “Kinetics of nucleotide-dependent structural transitions in the kinesin-1 hydrolysis cycle.,” *Proc. Natl. Acad. Sci. U. S. A.*, vol. 112, no. 52, pp. E7186-93, 2015.

[44] G. Y. Chen, K. J. Mickolajczyk, and W. O. Hancock, “The kinesin-5 chemomechanical cycle is dominated by a two-heads-bound state,” *J. Biol. Chem.*, vol. 291, no. 39, pp. 20283–20294, 2016.

[45] J. O. L. Andreasson, B. Milic, G. Y. Chen, N. R. Guydosh, W. O. Hancock, and S. M. Block, “Examining kinesin processivity within a general gating framework,” *Elife*, vol. 2015, no. 4, pp. 1–44, 2015.

[46] M. T. Valentine and S. M. Block, “Force and premature binding of ADP can regulate the processivity of individual Eg5 dimers,” *Biophys. J.*, vol. 97, no. 6, pp. 1671–1677, 2009.

[47] F. Kozielski, “Kinesins and cancer,” *Kinesins and Cancer*, vol. 12, no. August, pp. 1–271, 2015.

[48] A.-L. Salmela and M. J. Kallio, “Mitosis as an anti-cancer drug target.,” *Chromosoma*, vol. 122, no. 25, pp. 431–49, 2013.

[49] P. V Jallepalli and C. Lengauer, “Chromosome segregation and cancer: cutting through the mystery,” *Nat. Rev. Cancer*, vol. 1, no. 2, pp. 109–117, 2001.

[50] Y. H. Chi and K. T. Jeang, “Aneuploidy and cancer,” *J. Cell. Biochem.*, vol. 102, no. 3, pp. 531–538, 2007.

[51] I. Decordier, E. Cundari, and M. Kirsch-Volders, “Survival of aneuploid, micronucleated and/or polyploid cells: Crosstalk between ploidy control and apoptosis,” *Mutat. Res. - Genet. Toxicol. Environ. Mutagen.*, vol. 651, no. 1–2, pp. 30–39, 2008.

[52] R. W. King, “When 2 + 2 = 5: The origins and fates of aneuploid and tetraploid cells,” *Biochim. Biophys. Acta - Rev. Cancer*, vol. 1786, no. 1, pp. 4–14, 2008.

[53] A. C. Groen *et al.*, “A novel small-molecule inhibitor reveals a possible role of kinesin-5 in anastral spindle-pole assembly.,” *J. Cell Sci.*, vol. 121, no. Pt 14, pp. 2293–300, 2008.

[54] D. A. Skoufias *et al.*, “S-trityl-L-cysteine is a reversible, tight binding inhibitor of the human kinesin Eg5 that specifically blocks mitotic progression,” *J. Biol. Chem.*, vol. 281, no. 26, pp.

17559–17569, 2006.

[55] "No Title," *The Molecular Probes Handbook*, 2010. [Online]. Available: https://www.thermofisher.com/us/en/home/references/molecular-probes-the-handbook/tables/spectroscopic-properties-of-mant-atp-in-aqueous-solution-ph-8.html. [Accessed: 20-Jun-2015].

[56] M. Wieczorek, S. Bechstedt, S. Chaaban, and G. J. Brouhard, "Microtubule-associated proteins control the kinetics of microtubule nucleation.," *Nat. Cell Biol.*, vol. 17, no. 7, pp. 907–16, 2015.

ACADEMIC VITA

Colin Mark Lingafelt

Email: cql5356@psu.edu, colinlingafelt@gmail.com

EDUCATION

2015 - 2017	The Pennsylvania State University, Schreyer Honors College, University Park, PA B.S. Biomedical Engineering (May 2017) Chemistry Minor
2013 - 2014	The Pennsylvania State University, Honors Program Altoona, PA Pre-Engineering

RESEARCH EXPERIENCE

- **Student Researcher**, Department of Biomedical Engineering Penn State University (May 2015 - May 2017) PI: William O. Hancock, Ph.D.

  Developed cost-efficient protocol for synthesizing, purifying, and characterizing mant-labeled nucleotides to be used in mass producing fluorescent nucleotides for kinetics experiments and storage of molecular motors. Implemented imaging assay and polymerization assay techniques to assess the effect of kinesin motors on microtubule dynamics.

- **Research Assistant**, Department of Chemistry, Penn State University (Jan. 2014 - Dec. 2014) PI: Nan X. Xu, Ph.D.

  Performed synthesis reactions to create synthetic porphyrin models using a refluxing condenser and a nitrogen-gas vacuum line pump. Characterized porphyrin models using Nuclear Magnetic Resonance Imaging, Infrared Spectroscopy, and UV-VIS Spectroscopy. Implemented recrystallization techniques to interact synthetic porphyrin models with acrylamide and other reagents like nitric oxide.

PUBLICATIONS

- Six-coordinate Ferric Porphyrins Containing Bidentate N-t-Butyl-N-nitrosohydroxylaminato Ligands: Structure, Magnetism, IR spectroelectrochemistry, and Reactivity, N. Xu, J. Christian, N. Dalal, E. Abucayon, **C. Lingafelt**, D. Powell, G. Richter-Addo. *Dalton Trans.*, December 14, 2014, doi: 10.1039/C5DT03074A

PRESENTATIONS

- *Talk*: Interactions of Acrylamide with Synthetic Heme Models, **C. Lingafelt**, N. Xu, (April 2014) Penn State Altoona Undergraduate Research and Creative Activities Fair, Altoona, PA
- *Poster*: Synthesis and Solid State Molecular Structures of Five- and Six- Coordinate

Primary Amide Ferric Porphyrin Complexes, N. Xu, D. Powell, **C. Lingafelt**, G. Richter-Addo, (March 2015) ACS Biannual Meeting, Denver, CO

- *Poster*: Synthesis and Solid State Molecular Structures of Five- and Six- Coordinate Primary Amide Ferric Porphyrin Complexes, N. Xu, D. Powell, **C. Lingafelt**, G. Richter-Addo, (April 2015) Penn State Altoona Undergraduate Research and Creative Activities Fair, Altoona, PA

WORK EXPERIENCE

- BME 413 - Mass Transport of Biological Systems, Grader (Penn State University, 2017): Graded homework assignments and quizzes

- Student-Athlete Tutor - Morgan Center for Academic Excellence (Penn State University, 2015 - 2017): Aided Division I Athletes in their studies, Subjects tutored include - Calculus (I, II, and III), Algebra, Trigonometry, Physics (Mechanics and Electricity/Magnetism), General Chemistry, General Biology, and Physiology

SKILLS

- **Programming**: Design of data analysis programs; strong with MATLAB, familiar with signal/image processing
- **Microscopy**: Total internal reflection fluorescence microscopy (TIRF)
- **Imaging Techniques**: Nuclear magnetic resonance, infrared spectroscopy, UV-VIS spectroscopy, cyclic voltammetry, fluorescence spectroscopy
- **Experimental Procedures**: Microtubule imaging assays, spectrofluorometer protein kinetics measurements, spectrophotometer protein measurements, ATPase assay experiments, microtubule polymerization experiments, DEAE Sephadex Column protein purifications

HONORS/AWARDS

- Thompson Engineering Scholarship, Penn State (2016 - 2017)
- Schreyer Honors Scholar, Penn State (2015 - 2017)
- President Sparks Award, Penn State Altoona (2014 - 2015)
- Honors Program Scholarship, Penn State Altoona (2014 - 2015)
- President's Freshman Award, Penn State Altoona (2013 - 2014)

ACTIVITIES/MEMBERSHIPS

- Tau Beta Pi, National Engineering Honors Society, Vice President (2015 - 2017)
- Biomedical Engineering Society, Member (2015 - 2017)
- Penn State Altoona Division III Varsity Cross Country, Athlete (2014)
- Penn State Altoona Math Club, Member (2013 -2014)
- Mount Nittany Medical Center, Anesthesia Aide (2013)